Edward L. Ginzton Laboratory
W. W. Hansen Laboratories of Physics
Stanford University
Stanford, California

ACOUSTIC MICROSCOPY FOR NONDESTRUCTIVE EVALUATION OF MATERIALS

Semiannual Technical Report

for the period

1 August 1978 — 31 January 1979

Sponsored by
Advanced Research Projects Agency (DOD)
ARPA Order No. 3569
Monitored by NE Under Contract #F49620-78-C-0098

Principal Investigator: Professor C. F. Quate

G. L. Report No. 2956

SECURITY CLASSIFICATION OF THIS PAGE (When Data Entered)

REPORT DOCUMENTATION PAGE

READ INSTRUCTIONS BEFORE COMPLETING FORM

1. REPORT NUMBER

2. GOVT ACCESSION NO. AD-A148 536

3. RECIPIENT'S CATALOG NUMBER

4. TITLE (and Subtitle)

ACOUSTIC MICROSCOPY FOR NONDESTRUCTIVE EVALUATION OF MATERIALS

5. TYPE OF REPORT & PERIOD COVERED
Semiannual Technical Report
1 Aug. 1978 - 31 Jan. 1979

6. PERFORMING ORG. REPORT NUMBER
G.L. Report No. 2956

7. AUTHOR(s)

C. F. Quate

8. CONTRACT OR GRANT NUMBER(s)
F49620-78-C-0098

9. PERFORMING ORGANIZATION NAME AND ADDRESS
Edward L. Ginzton Laboratory
Stanford University
Stanford, California 94305

10. PROGRAM ELEMENT, PROJECT, TASK AREA & WORK UNIT NUMBERS

11. CONTROLLING OFFICE NAME AND ADDRESS
Advanced Research Projects Agency (DOD)
1400 Wilson Boulevard
Arlington, Virginia 22209

12. REPORT DATE
April 1979

13. NUMBER OF PAGES
50

14. MONITORING AGENCY NAME & ADDRESS (if different from Controlling Office)
Air Force Office of Scientific Research
Bolling Air Force Base
Washington, DC 20332

15. SECURITY CLASS. (of this report)
UNCLASSIFIED

15a. DECLASSIFICATION/DOWNGRADING SCHEDULE

16. DISTRIBUTION STATEMENT (of this Report)

"Approved for public release; distribution unlimited."

17. DISTRIBUTION STATEMENT (of the abstract entered in Block 20, if different from Report)

18. SUPPLEMENTARY NOTES

19. KEY WORDS (Continue on reverse side if necessary and identify by block number)

Acoustic microscopy
Imaging,
Materials
Integrated circuits
Non-destructive evaluation,
Silicon, and
Image enhancement,
Microprocessor

20. ABSTRACT (Continue on reverse side if necessary and identify by block number)

The progress in the program for acoustic microscopy is described for the preceding six month interval. The acoustic microscope working at 2.5 GHz has been used to study a variety of materials and a number of integrated circuits. We are beginning to see interesting features in these micrographs - features which are not evident in the optical images. Some of the effort has been spent on improving the instrument so as to extract particular and specified information of a given object. This is being done in part with the aid of a dedicated microprocessor. Originator-supplied Keywords include:

DD FORM 1 JAN 73 1473 EDITION OF 1 NOV 65 IS OBSOLETE

UNCLASSIFIED

SECURITY CLASSIFICATION OF THIS PAGE (When Data Entered)

TABLE OF CONTENTS

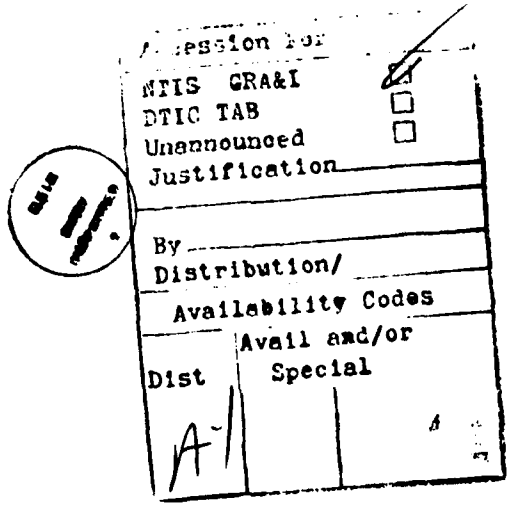

I. INTRODUCTION AND SUMMARY

During the first six months of this program on acoustic microscopy we feel that good progress has been made in three areas: 1) increased understanding of what can be measured with acoustic imaging, 2) improved electronic system for imaging with greater clarity, and 3) computer aided image enhancement. We have worked with both materials and integrated circuits. We have carried out further calculations on the profiles of the acoustic beam and we have been able to correlate much of this with measurements. The latter came from a new and simple method for recording the MTF. We now think that it is possible to penetrate the liquid-solid interface and focus the acoustic beam inside the body of a solid. If this system proves feasible it will give us a new power to explore the interior of materials on a microscopic basis.

We now have redesigned the microwave electronic systems used in conjunction with a new microscope working near 2 GHz and it is now being used to generate excellent images. We have achieved an improved signal-to-noise ratio and we have reduced some of the rf leakage that was producing a residual amount of interference.

We have incorporated a microcomputer into the output system and this enables us to store images in digital form on floppy discs. In turn we can transform these images into the spatial frequency domain. We are presently studying methods of filtering in this domain and we are searching for techniques that will give us enhanced images.

In parallel with this we have been recording images and studying the acoustic response of materials. We will include in this report our work with samples of brass, aluminum, and cobalt-titanium alloys. We are

interested in the appearance of grains and grain boundaries — the differences in elastic reflection of different material phases. We want to determine the most efficient method of presenting this information.

We have done extensive work on various devices furnished to us by the RCA Laboratories as fabricated with SOS technology and circuits fabricated on silicon in the Stanford Integrated Circuits Laboratory.

II. TECHNICAL CONTENT

(a) Modulation Transfer Function

We have continued our program for characterizing the acoustic beam that we are using as a probe. Our latest achievement is the realization of a new method for measuring the MTF of our acoustic system. It turns out to be rather simple and gives us new insight into the configuration of the beam.

We can analyze the problem with the imaging system as depicted in Fig. 1. It consists of a piezoelectric transducer at Plane 0, an acoustic lens with focal Planes 1 and 2 and the reflector object at Plane 3. The acoustic lens serves to focus the waves incident on Plane 1 and Plane 2. Using the similarity to an optical system a modulation transfer function can be defined. For this purpose one has to borrow from optics the assumption that the object acts like a "multiplicative" factor.[1] That is to say $u^-(x,y) = u^+(x,y) \times t(x,y)$ where u^+ is the incident field, t is the multiplicative object function and u^- is the reflected field. The validity of this assumption is questionable, because the angular spectrum of the field incident on the object is very broad ($\mp 50°$) as opposed to a narrow spectrum that is encountered in

[1] J.W. Goodman, Introduction to Fourier Optics (McGraw-Hill, New York, 1968), Chaps. 4-6, pp. 57-140.

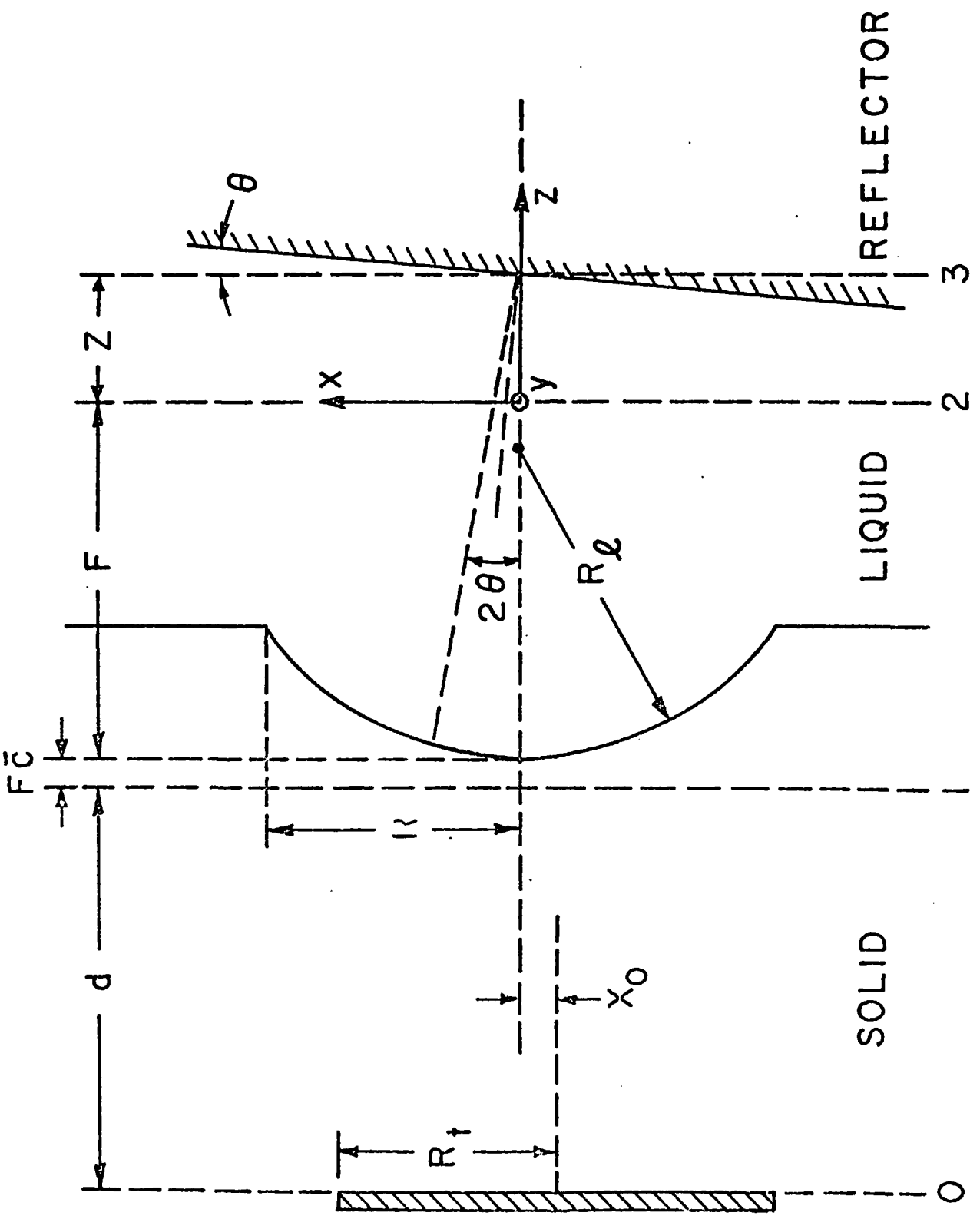

FIG. 1--Geometry and coordinate system used in analysis.

an optical system. This assumption neglects the fact that each plane wave component of the angular spectrum is treated differently by reflection process. Nevertheless it simplifies the theory to a level that the transfer function can be written as the convolution of the "generalized pupil function" with itself.[2] Therefore we write

$$\mathcal{H}(f_x,f_y) = K \iint_{-\infty}^{\infty} G(x,y)\, G(f_x\lambda_o F - x,\ f_y\lambda_o F - y)\, dxdy \qquad (1)$$

where f_x and f_y are spatial frequencies, K is a normalization constant, F is the focal length of the lens, λ_o is the wavelength in the liquid and G is the generalized pupil function. The transfer function is directly related to the resolution of the system and it takes the form of a "Chinese hat function" if G is a simple circular pupil.[1] G should include factors like the illumination of the lens at Plane 1 (u_1^+), transmission function at the lens surface and the pupil function. Hence we write $G(x,y) = u_1^+(x,y)\, P(x,y)$.

Note that the transfer function above is similar but not identical to that of an incoherent optical system. It does not necessarily have its maximum at $f_x = f_y = 0$ since G may not be circularly symmetric.

Now assume that there is a perfect reflector at Plane 3. In this situation the reflected field at Plane 1 can be written as[3]

$$u_1^-(x,y) \cong u_1^+(-x,-y)\, P(-x,-y)\, P(x,y)\, \exp[-jZk_o(x^2+y^2)/F^2] \qquad (2)$$

---

[2] R. A. Lemons, "Acoustic Microscopy by Mechanical Scanning," Ph.D. Dissertation, Stanford University (1975).

[3] A. Atalar, "An Angular Spectrum Approach to Contrast in Reflection Acoustic Microscopy," J. Appl. Phys. 49, 5130 (October 1978).

where the superscripts + and - refer to the fields propagating in +z and -z directions, respectively. Now let us tilt the reflector an angle θ with respect to Plane 3. Using the paraxial approximation one finds that the reflected field at Plane 1 is shifted laterally from its original position by $F \sin 2\theta \approx 2\theta F$:

$$u_1^-(x,y) \cong u_1^+(2\theta F-x,-y)\ P(2\theta F-x,-y)\ P(x,y)\ \exp\left\{-jZk_o[(\theta F-x)^2 + y^2]/F^2\right\}$$

Since the output of the transducer can be expressed as[3]

$$V = \iint_{-\infty}^{\infty} u_1^+(x,y)\ u_1^-(x,y)\ dxdy$$

we find

$$V(Z,\theta) \cong \iint_{-\infty}^{\infty} u_1^-(x,y)\ u_1^+(2\theta F-x,-y)\ P(2\theta F-x,-y)\ P(x,y)$$

$$\exp\left\{-jZk_o[(\theta F - x^2) + y^2]/F^2\right\} dxdy \qquad (3)$$

Comparing Eqs. (1) and (3), one concludes that

$$\mathcal{H}(f_x,0) \cong V(0,f_x\lambda_o/2) \ .$$

Therefore MTF can be found by measuring the output amplitude as a function of the tilt angle. A tilt angle of θ corresponds to a spatial frequency of $2\theta/\lambda_o$. It is obvious that by tilting the reflector in the y direction as well, one can generate the whole two-dimensional function. This tedious experimental procedure can be simplified if one uses a spherical

reflector,[4] since a sphere has a reflecting surface at all angles. The radius of the sphere must, of course, be much greater than the size of the focused beam.

A YIG sphere of diameter 380 microns is used as a reflector to measure MTF of a lens with parameters $R_\ell = 34$, $R = 29$, $R_t = 102$, $d = 2000$, $F = 39$, all in microns. First the YIG ball is moved in x and y directions (no z movement) until the time delay of the return pulse is minimized. This aligns the center of the ball with the lens axis. Then the ball is stopped in the x and y directions while the z position is adjusted each time for maximum return pulse amplitude. This amplitude is then recorded to generate the function $|\mathcal{H}(f_x,f_y)|$. In Fig. 2 the measured points are shown for a cross section of the function. We observe that MTF is not symmetrical about the origin which suggests that the illumination of the lens (u_1^+) is not centered correctly. This may arise from the misalignment of the transducer and lens axes (labeled X_o in Fig. 1) during fabrication.

Equation (3) can be generalized by including a reflectance function $\mathcal{R}$ as follows:

$$V(Z,\theta,\phi) \cong \iint_{-\infty}^{\infty} u_1^+(x,y)\, P(x,y)\, u_1^+(2\theta F-x,2\phi F-y)\, P(2\theta F-x,2\phi F-y)$$

$$\mathcal{R}(x/F-\theta,y/F-\phi)\, \exp\left\{-jZk_o[(x-\theta F)^2+(y-\phi F)^2]/F^2\right\} dxdy \quad (4)$$

where ϕ is the tilt of the reflector in the y direction.

[4] V. Jipson, private communication.

In Fig. 2 we also show MTF calculated by Eq. (4) where an offset X_o of 25 μ is assumed. The reflectance function $\mathcal{R}$ has negligible effect for $Z \simeq 0$, therefore $\mathcal{H}(f_x,f_y) \cong V(0,f_x\lambda_o/2,\ f_y\lambda_o/2)$ is a good approximation

An acoustic image of an aluminum surface recorded at 1500 MHz with the sames lens is presented in Fig. 3. The diamond mark is an "inverted pyramid indent" on the surface and the upper two faces are brighter than the two lower ones displaying the unsymmetrical nature of the MTF. The same argument can be used to explain the "shadowing" found in many acoustic images. This measurement also gives a direct feedback for the fabrication about the illumination of the lens and the alignment of the transducer.

(b) New Electronics

An entire new electronic system has been designed and constructed. It gives us an improved signal-to-noise ratio, an improved "on-off" ratio and shorter pulse lengths. These in combination will permit us to work with still smaller lens and this, in turn, should allow us to move to higher frequencies with improved resolution.

The electrical excitation circuitry is an important part of an acoustic reflection microscope system affecting the overall system performance. It must be designed carefully if interference-free images are desired. Most important, parameters in the design are the duration and on-off ratio of the input rf pulse.

The maximum allowable pulse duration is determined by considering the acoustic reflections inside the sapphire rod which has the lens on one side,

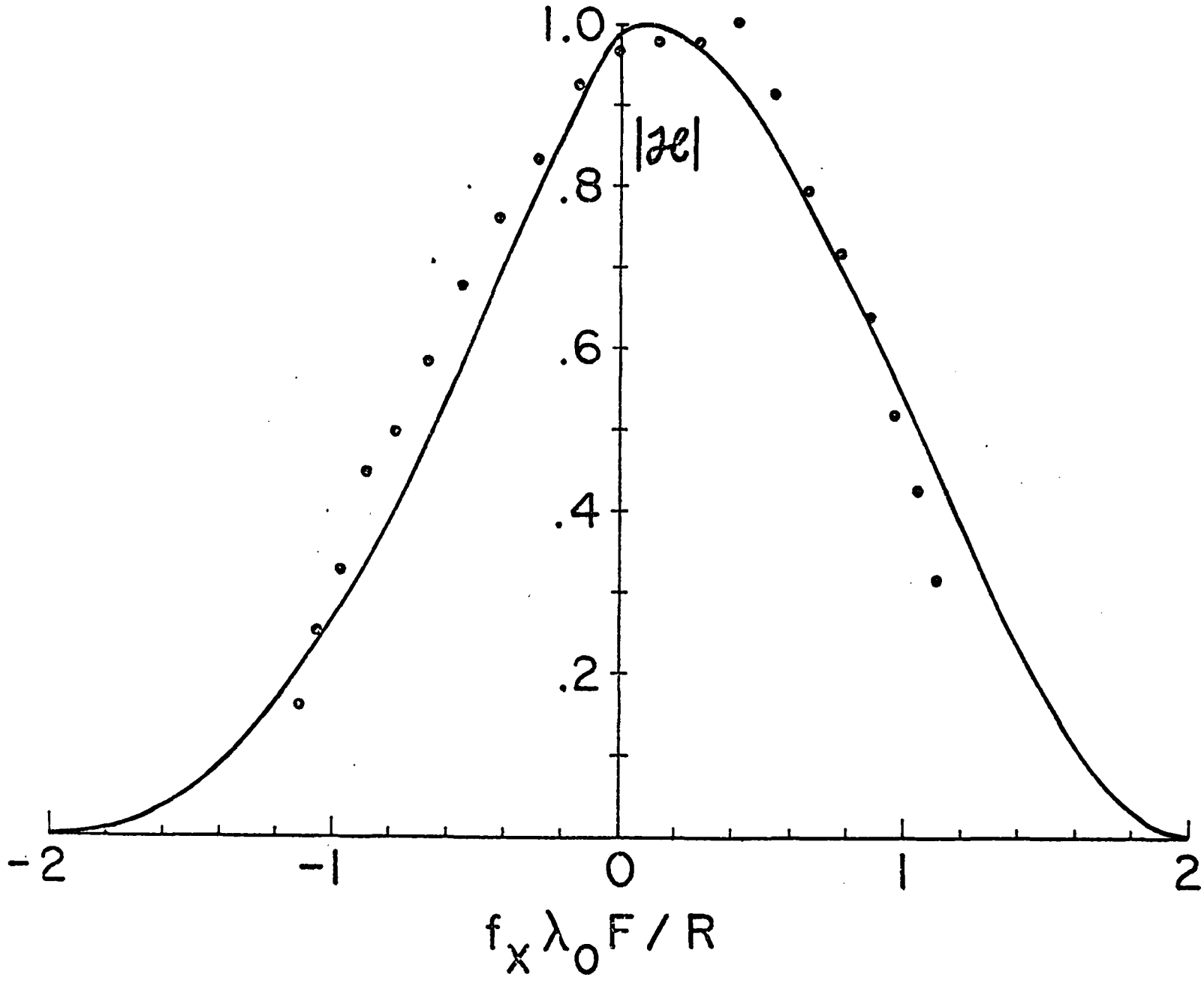

FIG. 2--Measured (dots) and calculated (solid l ne) m. or an acoustic microscope system.

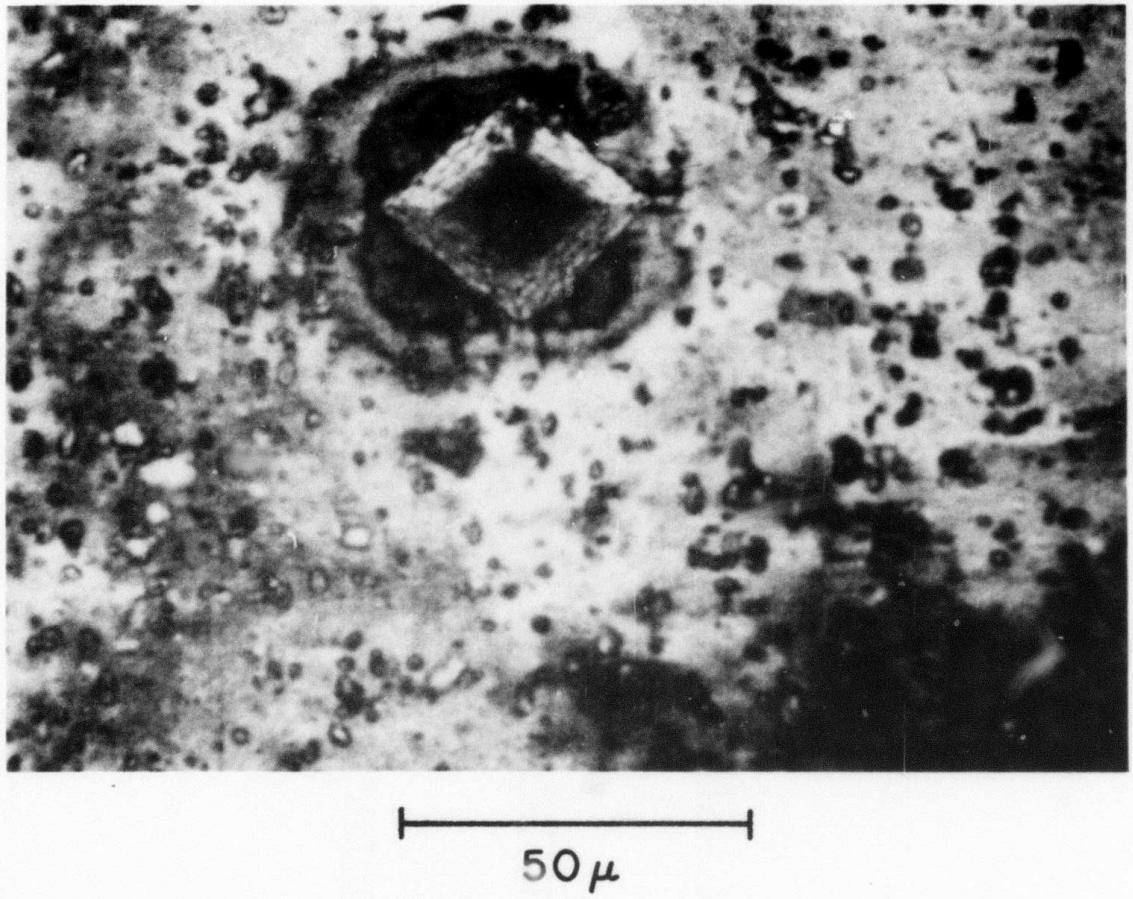

FIG. 3-- The surface of aluminum with a diamond-shaped indent. The uneven reflection from the sides of the indent are attributed to a non-symmetrical beam (see text).

the transducer on the other. The internal reflections are generated because of the fact that not all the energy transmitted by the transducer is fed into the liquid. For lenses with radius less than 100 microns, the most troublesome of these spurious reflections is the first internal reflection, since it is closest to the information pulse. In this case maximum pulse width is given by $2F/V_o$ where F is the focal length and V_o is the sound velocity inside the liquid. This criterion is valid for pulses with infinitely sharp edges. In reality, the pulse due to the first internal reflection has a finite fall time and moreover, it is much larger in amplitude than the information pulse. Therefore the pulse duration must be selected shorter — perhaps by a factor of 5 — than that given by $2F/V_o$. For example, the maximum allowable pulse duration for a 35 micron lens will be approximately 10 nsec.

The two methods that have been in use thus far for short pulse generation can be summarized as follows:

1) The output of a frequency generator set at the operating frequency is fed into a microwave switch. Turning on the switch for a short duration generates an rf pulse. The required good on-off ratio is achieved by a p-i-n diode switch. However, in this system the minimum pulse width is limited to about 10 nsec. For lenses smaller than 35 microns this is not acceptable.

2) A very short base-band pulse (500 psec) is used to excite the transducer. Since a short pulse contains frequencies till about the reciprocal of the pulse width (up to 2 GHz for 500 psec pulse), an excitation is possible. This method can be thought of as measuring the "impulse response" of the system. Consequently the output pulse width is determined by the system bandwidth — the shortest pulse width possible. This method fails above 2 GHz when it becomes difficult to obtain pulses shorter than 500 psec with reasonable amplitude.

For an instrument utilizing a 35 micron lens and operating 2 GHz, or higher frequencies, the new excitation scheme described below is preferred. This method utilizes a "voltage controlled oscillator (VCO)" as the rf source. Referring to Fig. 4, assume that a ramp is applied to the frequency control of a VCO and that a band-pass filter (BPF) is connected to the output of it. As the frequency is swept through the bandpass of the filter, a pulse will be generated at the BPF output. This pulse will be in the form of an rf chirp and its duration will be set by sweep-rate as well as bandwidth of BPF. For example, a shorter pulse can be generated if the sweep rate is increased. Note that there is a limit to this since output pulse width cannot be any shorter than the reciprocal of the bandwidth of BPF. The on-off ratio of the pulse is determined by stop-band attenuation of BPF. At first this may seem unacceptable, but notice that the leakage signal has a frequency far different than the pulse center frequency and hence will not cause any interference.

As a VCO we consider the "varactor tuned oscillators (VTO)". Their ability to sweep the frequency at a fast rate makes them a good choice. Typically a VTO centered at several gigahertz can sweep through 1 GHz range in about 30 nsec with a step voltage applied to its frequency control input.

An acoustic microscope system is built using the technique described above. A block diagram of the system is shown in Fig. 5. A VTO covering the range 1.5 — 2.7 GHz is selected. A bandpass filter at 2 GHz with a bandwidth of 400 MHz is designed and built using the coupled $\lambda/2$ ssections on a microstrip board. This is followed by a Class A and a Class C amplifier. The Class C amplifier consisting of a microwave transistor on a microstrip board has 1.5 W power output capability. It helps to increase the on-off

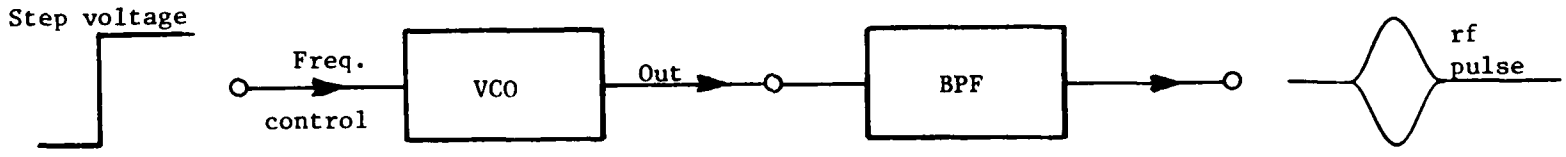

FIG. 4 The schematic showing the method of generation of the short r.f. pulse.

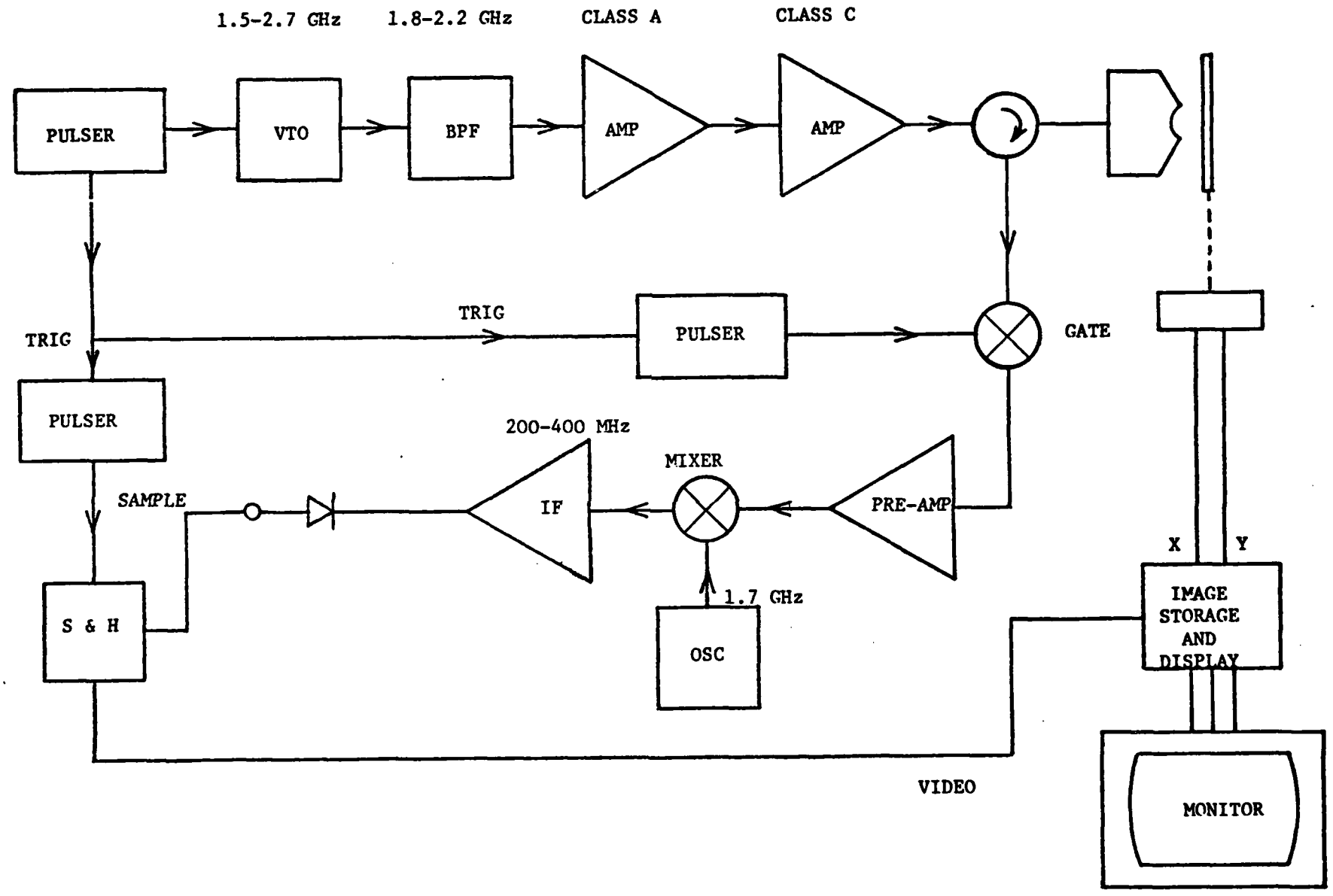

FIG. 5--Block diagram of the electronic system.

ratio, since it has a very small gain for low level signals. This system generates a 1.5 W 10 nsec pulse at 2 GHz which is fed into the acoustic cell. The return pulse from the object is first preamplified and then mixed down to an IF frequency at 300 MHz. IF selectivity provides the necessary on-off ratio by rejecting the frequencies other than 2 GHz. A signal-to-noise ratio of 30 dB is obtained with water temperature around 40 — 50°C. At 2 GHz the wavelength in water is 0.75 microns and a resolution of 0.6 microns is estimated.

(c) Image Storage and Enhancement

We have incorporated a Cromenco minicomputer into the instrument complete with A-D converters and image storage on floppy discs. An example of a stored image is shown in Fig. 6 together with the image as recorded directly with analog signals.

Since there are several acoustic microscopes existing within our labs, it is desirable that any image storage system be easily duplicated and inexpensive. With these goals in mind, an 8-bit microprocessor system (Z-80 based) was employed to construct a digital image storage system. As presently implemented the system stores acoustic micrographs on single density floppy discs as an array of 256 × 256 pixels with each pixel recorded to 8-bit accuracy. Each pixel is recorded as a single byte since: 1) it alleviates the need for data packing schemes, and 2) it allows the total signal-to-noise ratio (up to 45 dB) of the microscope to be recorded. The image is recorded as 16 tracks each of which is 4 kbytes long. Interrupt driven disc I/O is utilized to make the storage system compatible with the

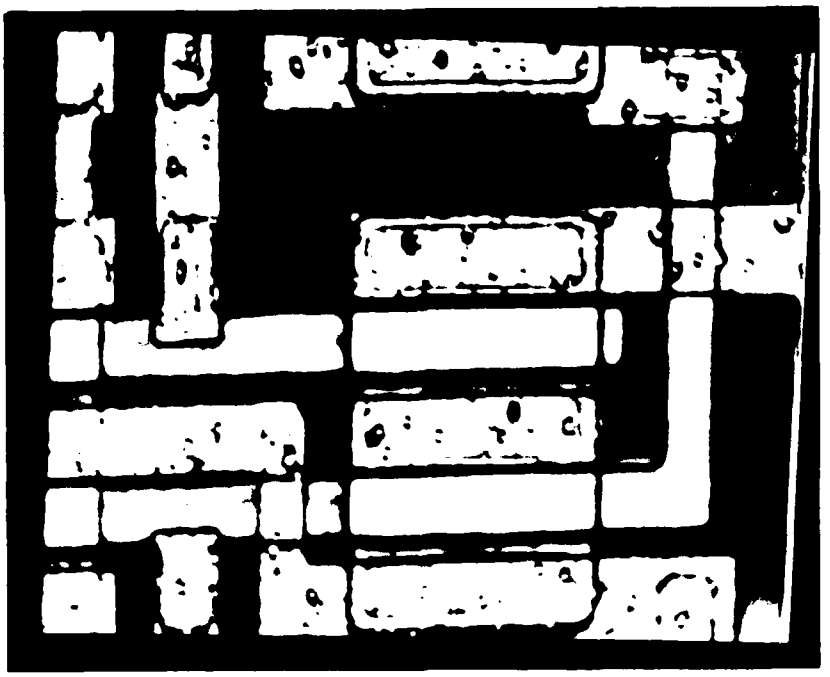

(a)

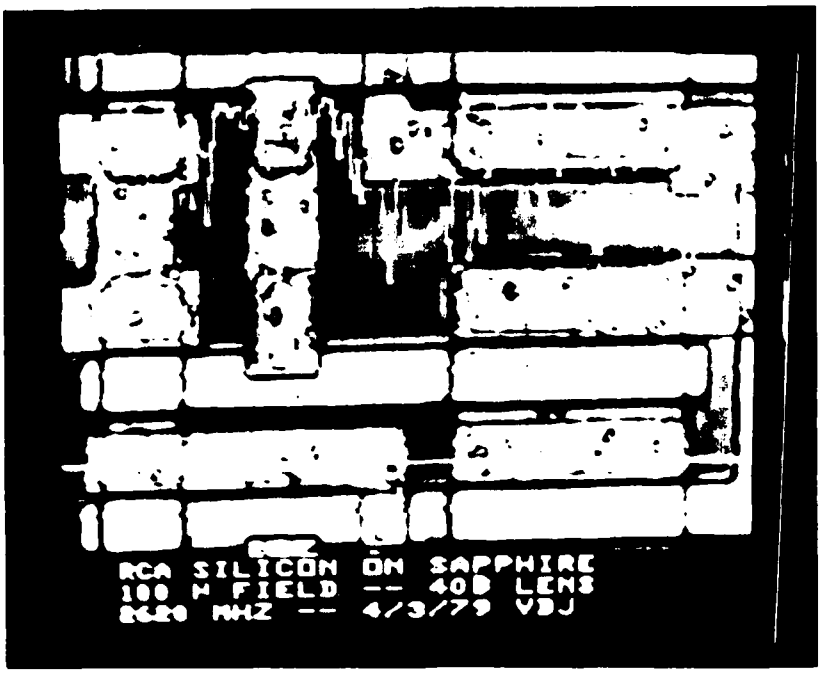

(b)

FIG. 6--The direct analog image of an SOS circuit in (a) and the image after storage on a floppy disc (b).

frame time of the microscope. Using this format 8 images can be stored on a dual sided floppy disc. Only intensity information is stored since position information can be readily synthesized by the microcomputer. The image is displayed by outputting it line by line to a scan converter which then interfaces directly with a television monitor.

The storage system is build around a Cromenco Z-2 microcomputer system containing 48K RAM and dual eight-inch floppy disc drives. With the exception of a real time input port used to collect data from the microscope, a hardware 16-bit multiply[5] board used to increase computational speed and the software the whole system is commercially available. A Z-80 based system was chosen primarily for the increased speed available with the 4 MHz clock.

Our motivation for digitally storing acoustic micrographs was to allow us to implement various image enhancement and restoration algorithms. As a first approach to restoration a spatial frequency approach using a Wiener filter was decided upon. This is a classic image restoration technique when the transfer function of the instrument can be either calculated or measured. If the transfer function of the instrument is $H(f_x,f_y)$ where (f_x,f_y) are the spatial frequency components, then the Wiener filter is given by:

$$F(f_x,f_y) = \frac{H(f_x,f_y)}{|H(f_x,f_y)|^2 + N(f_x,f_y)} \qquad (5)$$

where $N(f_x,f_y)$ is a two-dimensional statistical representation of the system noise in the spatial frequency domain. For the microscope the noise is assumed

[5]This board was designed and constructed by Bob Bray.

to be white. The restoration is performed by taking the two-dimensional Fourier transform of the image, multiplying it by $F(f_x,f_y)$ and inverse Fourier transforming.

The above technique, although straightforward, is difficult to implement on an 8-bit microcomputer system which does not have sufficient memory to store the entire image. The transform is performed as 256 row transforms followed by row-column interchange and 256 more row transforms. Each row consists of 256 points and a fast Fourier transform algorithm written in Z-80 assembly language performs the transforms. The speed of this operation is enhanced by the 16-bit hardware multiply board (less than half a second per 256 point transform). The total image enhancement algorithm takes approximately 10 minutes.

Our initial results show that it is indeed possible to achieve some enhancement of these images and we hope to include some examples in the next technical report.

(d) Material Studies

In Fig. 7 we present another image recorded with the new system. It is the surface of a brass sample that has been imaged earlier at lower frequencies. The same contrast mechanism is valid here that differentiates between the various phases of the alloy. Grain boundaries are easily seen with the increased resolution.

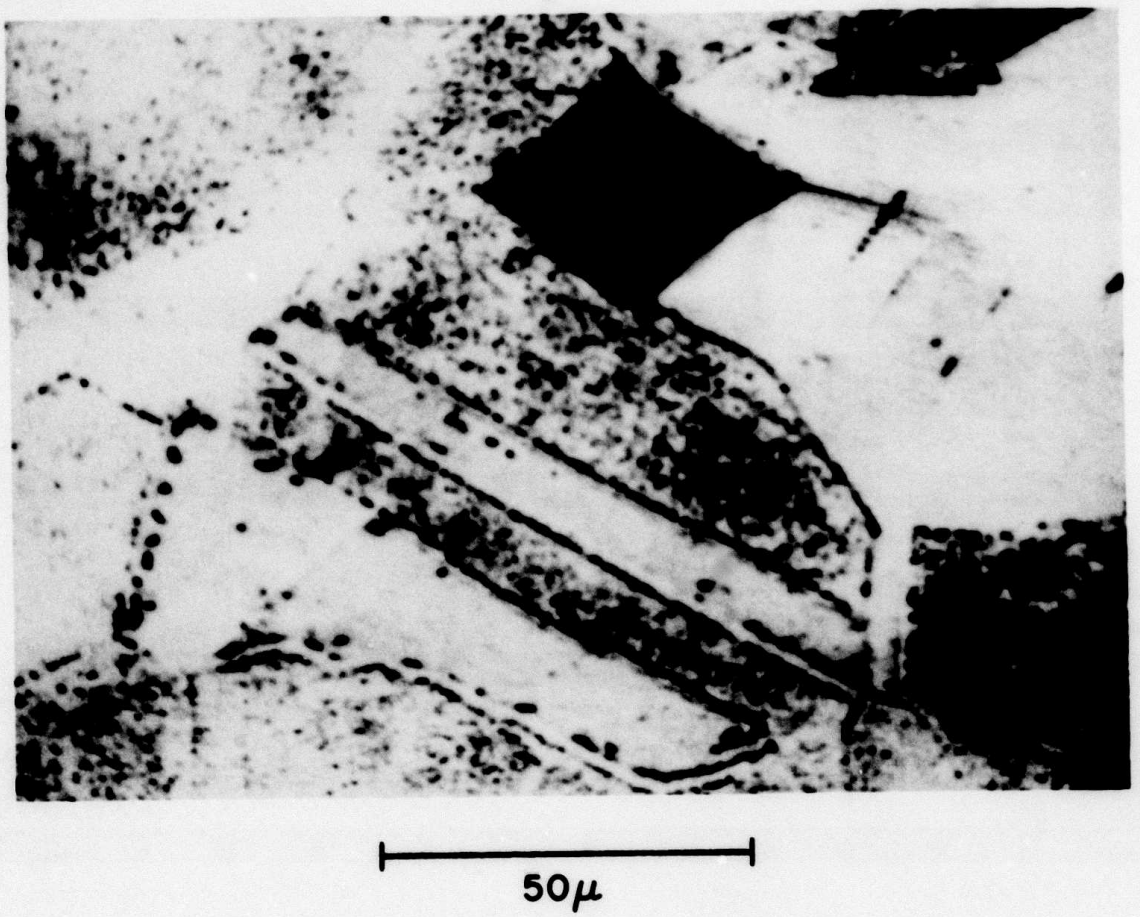

FIG.7--Acoustic image of a brass sample (f = 2 GHz).

In Fig. 8(A) another acoustic image of the surface of a brass sample is shown. The diamond mark is used for identification purposes. In this image, too, the different grains are easily separated.

For images that have low contrast, a different display technique can be used. This technique — known as composite A scan — uses the video signal to modulate Y input rather than the usual Z-intensity input. One obtains a one-line A-scan if the mechanical y motion is stopped. But then the individual A scans are displaced slightly in the y-direction for the successive lines. The resulting image of Fig. 8(B) has a "three-dimensional look" even though we have a two-dimensional image to start with. To improve the quality of the image, the video signal can be fed into Z input as well as Y input. This addition enhances the depth feeling even further.

(e) The V(Z) Curves — A Simple Interpretation

In previous publications, Atalar has described a method[3] whereby some of the elastic properties of the specimen can be determined by monitoring the output from the transducer as a function of the spacing between the lens and the reflecting surface. There is a certain periodicity in these curves which can be expressed with a simple function. Recently Weglein[6] has published experimental data relating to this periodicity for a wide variety of materials. In this section we want to develop the expression as taken from our previous publication[7] for this periodicity and show that it can be used to predict the values as measured by Weglein.

---

[6] R. D. Weglein, Appl. Phys. Lett. 34, 179 (1979).

[7] A. Atalar, "Acoustic Reflection Microscope," Ph.D. Dissertation, Stanford University (December 1978).

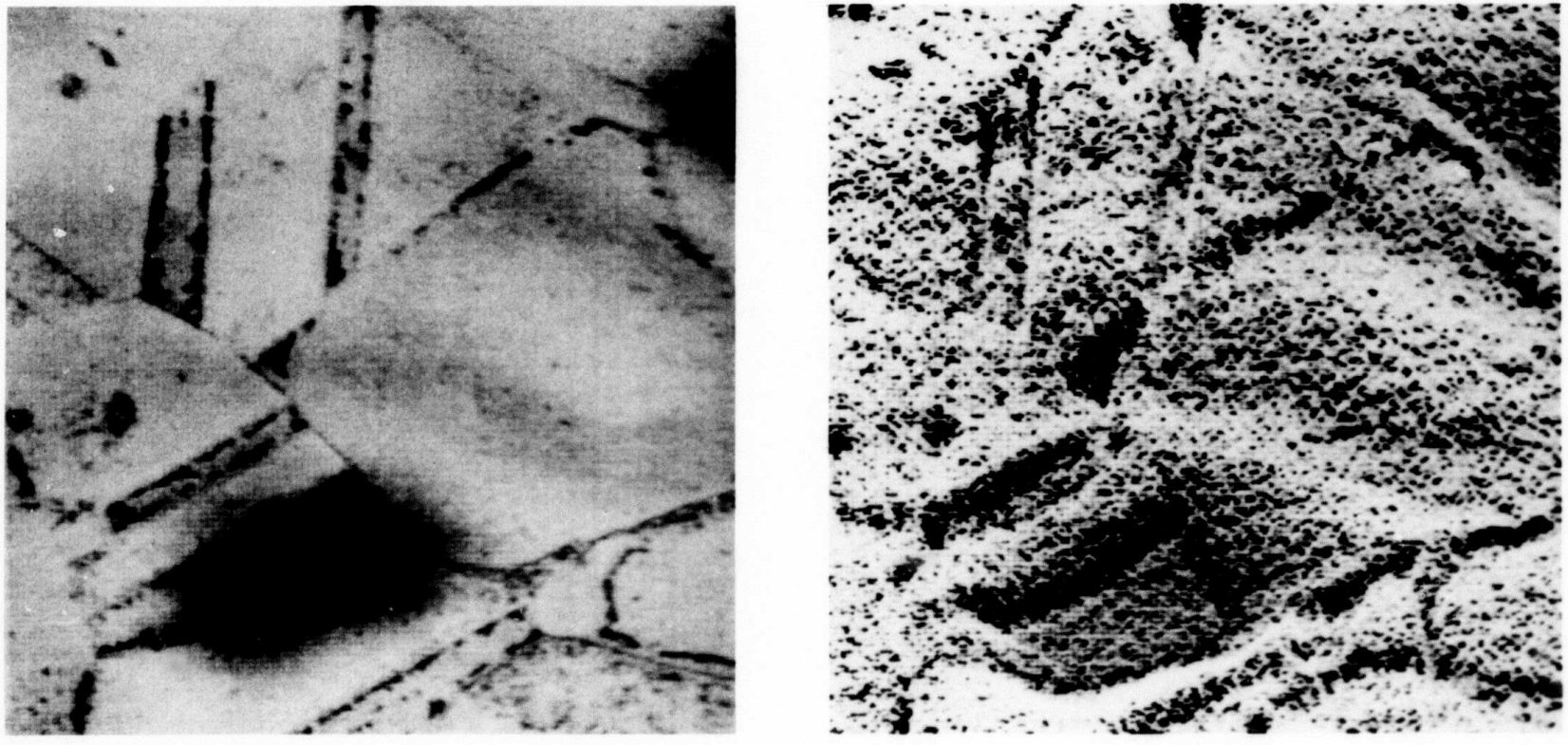

(A) (B)

FIG. 8- Acoustic images of a brass sample with (A) conventional raster scan and (B) composite A-scan displays.

We have learned from our work with the acoustic microscope that the reflectance function as transferred to the reflected wavefront can be revealed to the outside world by translating the object through the focused beam and recording the transducer output voltage. We have seen several examples of $V(Z)$ curves corresponding to different reflector objects. Those curves are unique to each material and therefore we can treat them as "signatures" of these materials. Most of the $V(Z)$ curves have peaks and dips, the distance between which changes with the acoustic parameters of the object. In this section we will try to understand the reason behind this.

The reflected field at the back focal plane of the acoustic lens can be expressed in the form when circular symmetry exists

$$u_1^-(r) = u_1^+(r)\, P^2(r)\, \mathcal{R}(r/f)\, \exp\left[j2k_o Z\sqrt{1-(r/f)^2}\right] \qquad (6)$$

where some constant factors are neglected.

Suppose that $u_1^+(r)\, P^2(r)\, \mathcal{R}(r/f)$ is purely real. For $Z = 0$ the wavefronts of the reflected wave will be parallel to the transducer. In this situation the transducer output will be maximum, for the wavefronts are parallel to the transducer. However if $Z \neq 0$ the wavefronts will have a curvature given by the exponential factor in (6). The output voltage is reduced since the wavefronts are tilted with respect to transducer. The main contribution to the output voltage comes from the region where the wavefronts are more or less flat. Examining the exponential factor shows that this is around $r \cong 0$.

We have previously investigated the behavior of the reflectance function for single crystal reflectors. If water is selected to be the liquid medium the amplitude of the reflectance function is very close to one for most materials.On the other hand, the reflectance function phase has a transition which varies considerably from material to material. This transition occurs at the Rayleigh critical angle which is determined by the Rayleigh wave velocity in the medium.

Now let us include this reflectance phase into our consideration. At $Z = 0$ the wavefronts will be tilted only for the region around $r/f = \sin \theta_R$. This is demonstrated in Fig. 9 by the wavefront A. The transducer will generate a large output since most of the wavefront is parallel to the transducer. When $Z = Z_1$ we must add the exponential factor of (6) which tilts the wavefront as shown by B in Fig. 9. For this case we expect to have two main contributing regions: One is around $r \simeq 0$ (1) and the other for $r \simeq f \sin \theta_R$ (2). The second region is created by the fact that the wavefront tilt due to the exponential factor partially cancelled the wavefront tilt due to the reflectance function. The transducer output voltage can be found by adding the two contributions vectorially. Therefore the phase relationships between these two quantities must be considered. If they are in phase they will add up to give a peak, but if they are out of phase there will be a dip. To have a peak the phase difference between (2) and (1) should be $2n\pi$ $(n=1,2,\ldots)$. Therefore we write

$$2k_c Z_1 \sqrt{1 - (r/f)^2}\,\Big|_{r=f \sin \theta_R} - 2k_o Z_1 \sqrt{1 - (r/f)^2}\,\Big|_{r=0} \cong 2n\pi \qquad (7)$$

From this we find

$$Z_1 \cong \frac{n\lambda_o}{2(\cos \theta_R - 1)} \qquad n=1,2,3,\ldots \qquad (8)$$

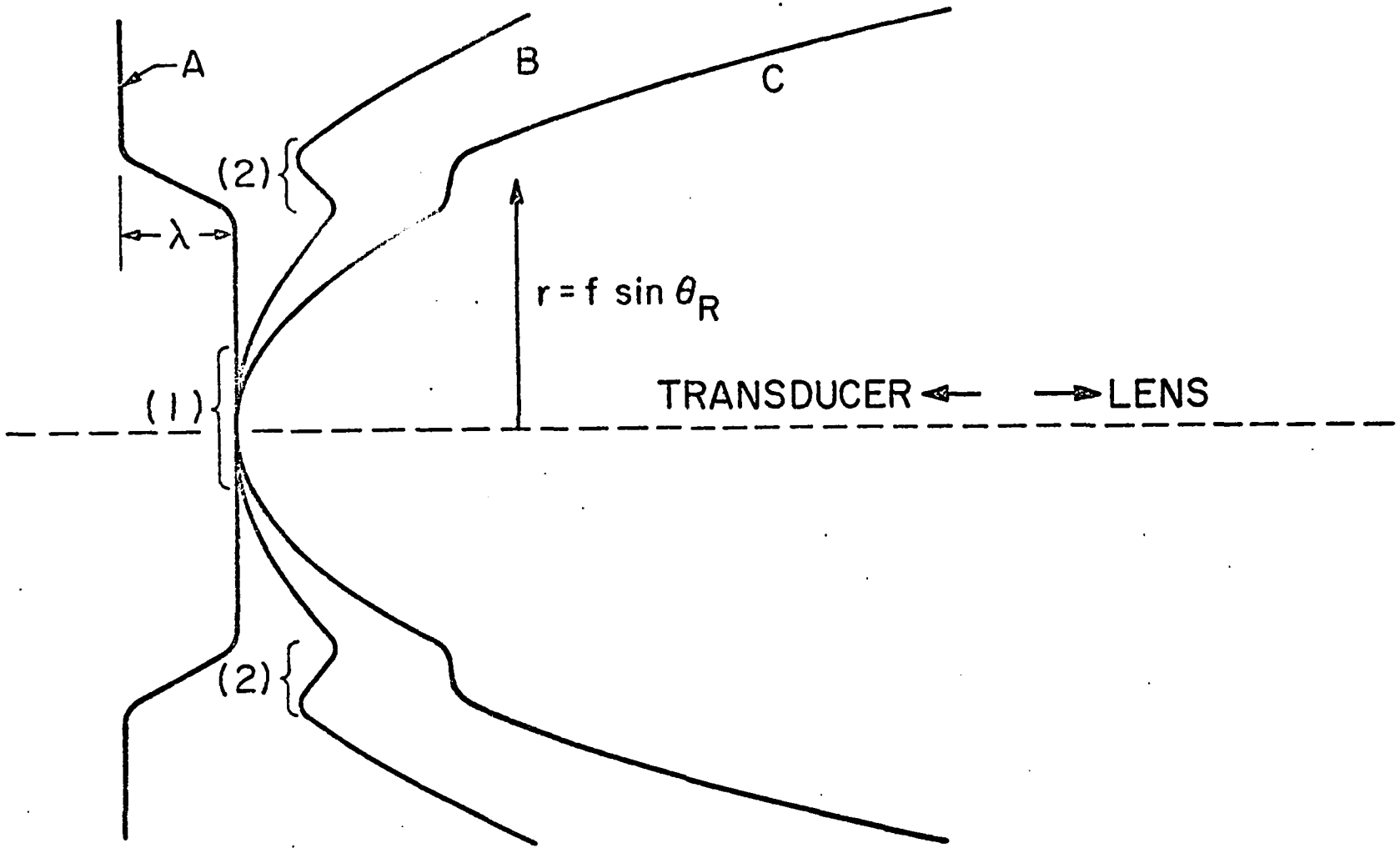

FIG. 9--The shape of the reflected wavefronts at the back focal plane of the lens for a single crystal reflector. Wavefront A is for Z = 0 . Wavefronts B and C are for increasingly negative values of Z .

Therefore the distance between the successive peaks is given by

$$\Delta Z \cong \frac{\lambda_o}{2(\cos \theta_R - 1)} \quad .$$

This simple relationship gives the distance between the peaks (or the dips) in terms of the wavelength and of the Rayleigh angle. It can be easily seen that the larger the Rayleigh angle, the closer will be the peaks. Since the Rayleigh angle is very close to the shear critical angle the shear velocity of the reflecting object is the dominant factor.

If $v_{liq}/v_{shear} \cong \sin \theta_R$ is greater than R/f, we do not expect to see any dips or peaks since the Rayleigh angle lies outside of the converging illuminating beam. For this case where all of the incident energy is reflected without a change in phase (an ideal mirror), we still find that the transducer output is a function of the spacing between the lens and the reflector. The details for this case has also been worked out by Atalar[7] and he finds that the response varies as $\sin x/x$ where $x \equiv (\pi/\lambda_o)(R/f)^2 Z$. Thus the distance between nulls, $\Delta Z' = \lambda_o (f/R)^2$ and for Weglein's case this number turns out to be about 10 microns.

Weglein[6] has measured ΔZ for a number of materials at 375 MHz with the results as in Fig. 10. The predicted value from Eq. (9) is also plotted there where we see that the agreement is close enough to give us confidence in this model.

(f) Imaging with High Velocity Liquid Metals

Since its introduction in 1973,[8] the scanning acoustic microscope has been utilized to examine acoustically thin objects in the transmission mode

[8] R. A. Lemons and C. F. Quate, Appl. Phys. Lett. 24, 163 (1974).

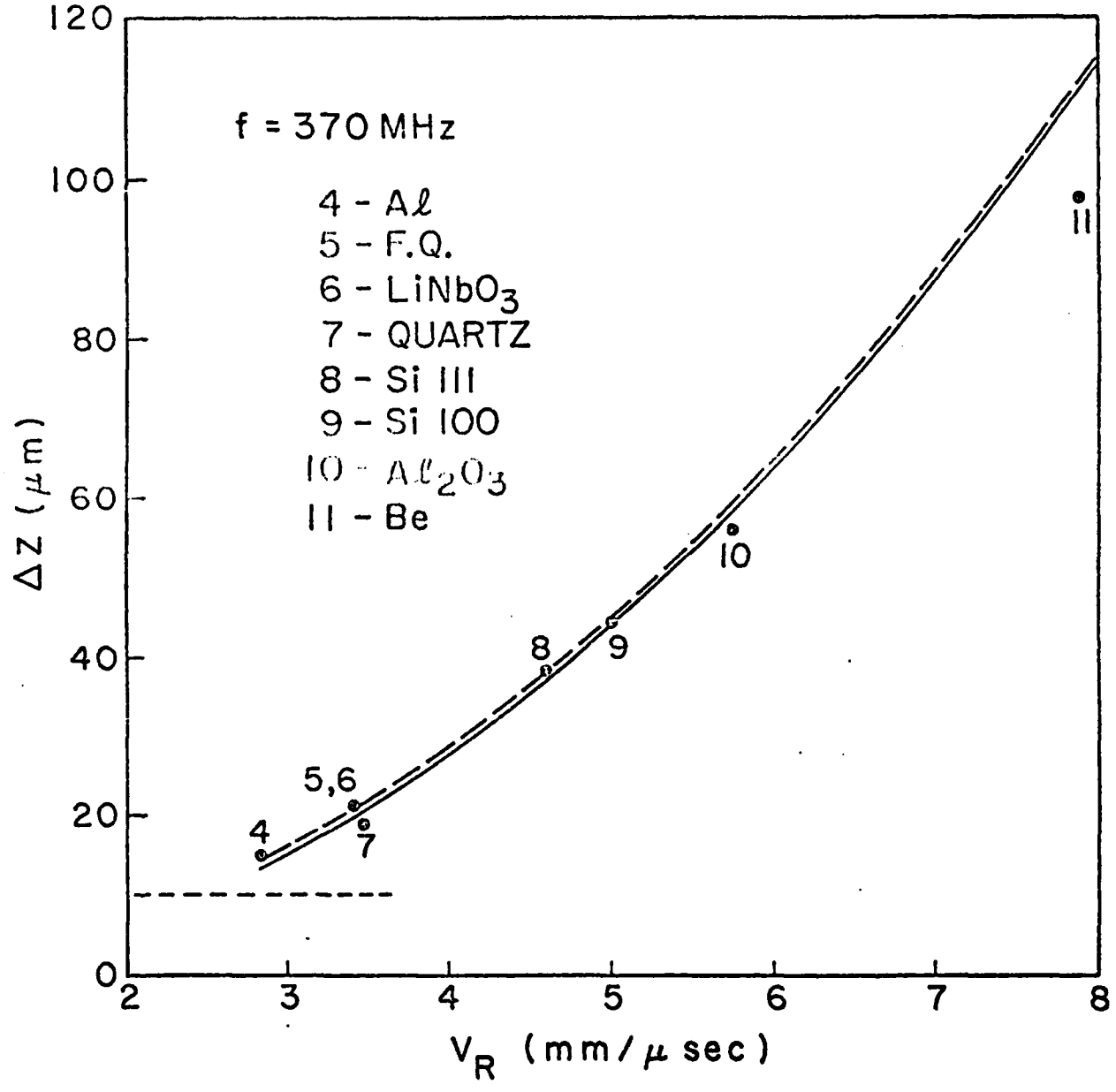

FIG. 10--The distance between minimum, ΔZ, on the V(Z) curve versus the Rayleigh velocity, V_R. (after Weglein).

and the surface regions of thicker samples in the reflection mode. For a more complete description of the acoustic microscope and its applications the reader is referred to previous work.[9] We will discuss here the possibility of using the acoustic microscope to examine planes inside an isotropic solid to a depth on the order of the lens radius with a resolution that is diffraction limited. This is accomplished by considering the use of the liquid metals as the coupling liquid and by taking advantage of mode conversion at the liquid-solid interface. The theoretical performance of the microscope in this mode of operation is examined.

The use of the acoustic microscope to examine the interior of materials or to "look" through materials has not received a great deal of attention. One notable exception to this is the work of Tsai[10] who has utilized a standard low frequency (150 MHz) acoustic microscope to image the interior of some objects. One of the motivations for using ultrasound for imaging is the "acoustic transparency" of most materials to ultrasound. Diffraction limited imaging inside the material presents difficulties that are not encountered when using the acoustic microscope to image surfaces or thin objects. First, the acoustic impedance mismatch between most liquids (water being the liquid normally used in the microscope) and solids is such that only approximately 10% of the acoustic energy will penetrate into the solid. Secondly, the ratio of the acoustic velocity in the liquid to that in the solid is typically low and thus upon entering the solid the acoustic energy

---

[9] V. B. Jipson and C. F. Quate, Appl. Phys. Lett. 32, 789 (1978).

[10] C. S. Tsai, S. K. Wang, and C. C. Lee, Appl. Phys. Lett. 31, 317 (1977).

is strongly refracted in such a way as to produce aberrations in the image.

These problems aside, we wish to consider the imaging performance of the microscope as shown in Fig. 11. This is identical to a normal reflection scanning acoustic microscope except that an isotropic solid has been introduced at a distance Z inside the focal length F_o of the acoustic lens. We want to calculate the distribution of acoustic energy at various depths within this solid so that we may understand the imaging inside the solid. With the ray tracing approach as in Fig. 11 we see that rays with low angles of incidence θ cross the lens axis at greater depths than do rays with large angles. This results in a focus aberration within the solid proportional to the distance $f - F_o$. By applying Snell's law at the lens-liquid and liquid-solid interface this aberration can be shown to be:

$$A(\theta) = \frac{f_o - f}{R} = \left[\frac{1}{1-\bar{C}} - \left(\frac{\sin\theta}{\tan(\phi)} + 1. - \cos\theta\right)\right] + \left[\frac{Z}{R}\frac{V_2}{V_3}\left(1. - \frac{\cos\phi'}{\cos\phi}\right)\right] \quad (10)$$

where

$$\bar{C} = \frac{V_2}{V_1}, \quad \theta' = \sin^{-1}\left\{\frac{V_2}{V_1}\sin\theta\right\}, \quad \phi = \theta - \theta', \quad \phi' = \sin^{-1}\left\{\frac{V_3}{V_2}\sin\phi\right\}, \quad (11)$$

V_i is the acoustic velocity of the corresponding material and all other quantities are defined in Fig. 11.

The first term in this expression is the usual spherical aberration term for the acoustic lens[2] while the second term is an additional aberration due to the refraction at the solid boundary. If these aberrations are small we expect a focus to occur within the solid at a depth $z = Z \times V_2/V_3$. The aberration for the lens itself is always positive

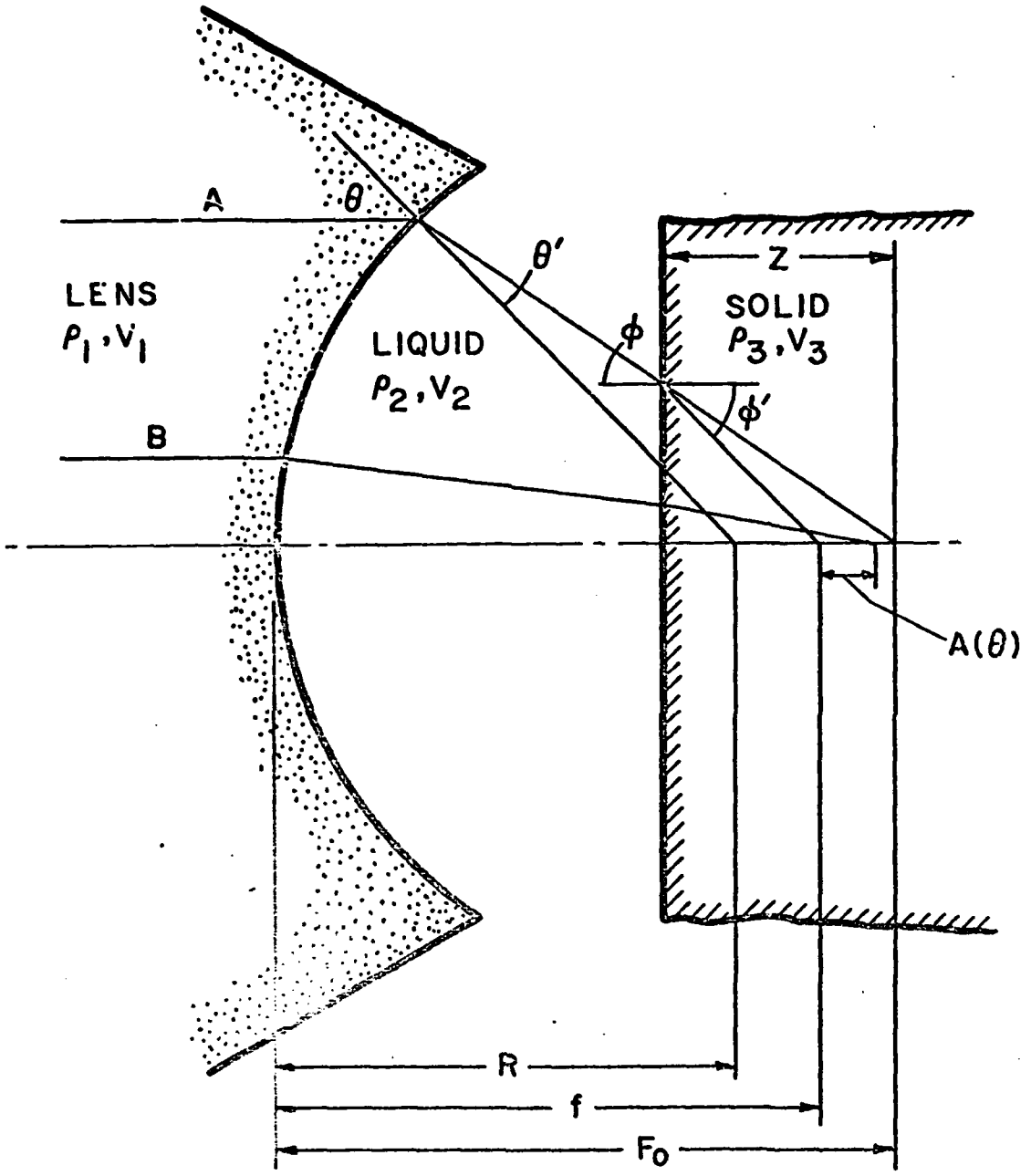

R = LENS RADIUS

F_o = LENS FOCAL LENGTH

Z = DISTANCE OBJECT IS DISPLACED TOWARD LENS

f = FOCAL LENGTH INSIDE THE OBJECT

FIG. 11--Geometry of the acoustic microscope as used in the internal focusing mode. ρ_i refers to the medium density and V_i to the appropriate acoustic velocity.

as defined here and increases as a function of θ . The additional aberration due to the inserted object is proportional to the normalized depth of penetration Z/R and will increase as a function of ϕ . If the acoustic velocity in the solid is less than the velocity in the liquid this aberration term will be negative. It can act to cancel the aberration of the lens itself. If $V_3 = V_2$, then $\phi = \phi'$ and there are no additional aberrations due to the object. The greater the velocity mismatch between the liquid and the solid, the larger will be the aberration due to the liquid-solid interface.

The limitations imposed by water as the coupling liquid (large velocity and mechanical impedance mismatch), do not arise with liquid gallium. Gallium offers three advantages: (1) its mechanical impedance of 16.9×10^5 g/sec-cm^2 is similar to that of most solids with the result that the liquid-solid boundary becomes essentially transparent, (2) its acoustic velocity of 2.87×10^3 m/sec as compared to 1.5×10^3 m/sec for water is a better match to most materials, and (3) it has low acoustic loss ($\alpha/f^2 = 1.58 \times 10^{-17}$ sec^2/cm) as compared to H_2O. The low loss will allow the microscope to be operated at frequencies of several GHz. Gallium does alloy with some materials and these must be excluded. Liquid mercury also has low loss, good mechanical impedance match and a velocity of 1.5×10^3 m/sec. It would be suitable for examining materials with low acoustic velocities but there is a difficult wetting problem with mercury.

The acoustic velocity of gallium is much larger than that of water, but it is still lower than the longitudinal acoustic velocity of most solids. However, the shear wave velocity in many solids is less than the velocity in gallium. This can (under certain circumstances) result in smaller focal plane abrerations than would be found if the object were not present. The

reduced shear wave velocity also implies a smaller acoustic wavelength, with an improvement in the resolution.

The major problem with this suggestion is the efficiency of the mode conversion from the incident longitudinal energy to the shear energy at the boundary. In order to evaluate the possibility of converting a reasonable amount of energy into shear waves, we will calculate the partition of acoustic energy inside the solid as a function of the incident angle of the longitudinal wave. This problem has been treated by several authors.[11] In Fig. 12 the percentage of reflected longitudinal, transmitted longitudinal and transmitted whear energy as a function of the incidence angle is shown for both a water-steel boundary and a gallium-steel boundary. It can be seen for the water-steel boundary that 80 - 90% of the incident energy is reflected as a longitudinal wave. At low angles of incidence approxiately 12% is transmitted as a longitudinal wave. For the gallium-steel case the situation is quite different. For low angles of incidence nearly 80% of the energy is transmitted as a longitudinal wave while above the longitudinal critical angle (ϕ = 29.7°) almost 100% is converted into the transmitted shear waves. Shear waves are most efficiently excited when the angle of incidence is above the longitudinal critical angle. The acoustic lens generates an angular spectrum of plane waves impinging upon the object with the maximum angle of incidence slightly less than the maximum opening angle of the lens itself.

A measure of the imaging potential inside materials using this technique can be obtained by considering the geometric aberrations of Eq. (10). A more rigorous approach is to calculate the acoustic field distribution inside the object as a function of depth. This can be accomplished by using an angular

---

[11] L. M. Brekhovskikh, Waves in Layered Media (Academic Press, New York, 1960), pp. 15-36.

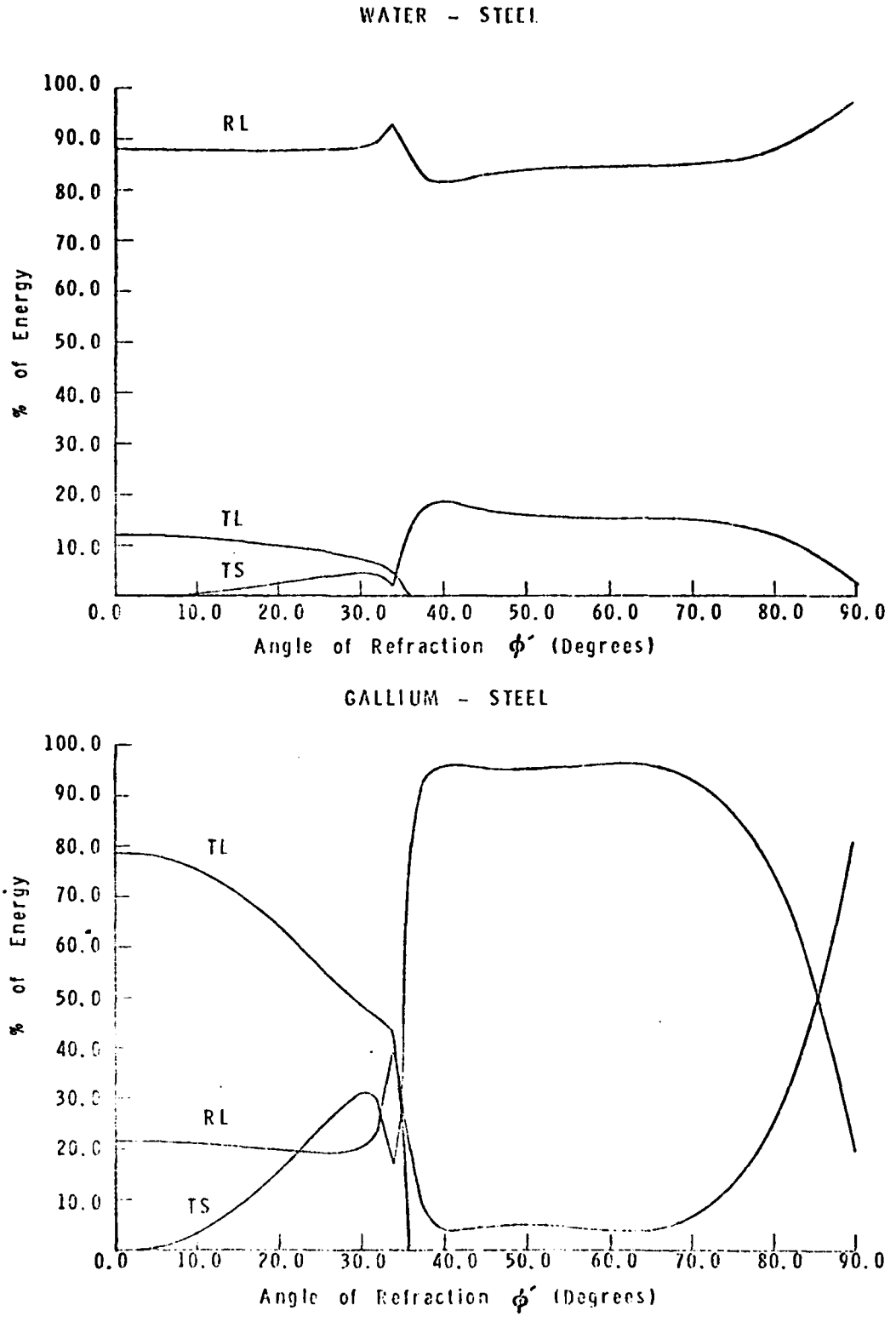

FIG. 12--Calculation of the acoustic energy partition into various modes for an incident longitudinal wave from the liquid onto the solid. RL is the reflected longitudinal energy, TL is the transmitted longitudinal energy and TS is the transmitted shear energy.

spectrum approach[3] and incorporating the acoustic transmission function at the liquid-solid interface. The results for this calculation for a gallium-steel geometry are shown in Fig. 13 for both the shear and longitudinal wave cases. Both calculations were performed for a paraxial focal depth of 100 μm inside the material (Z/R = 0.5) and for planes 4 acoustic wavelengths either side of this plane. The maximum opening angle θ of the lens was taken to be 30 degrees. For the shear wave case the 3 dB acoustic beamwidth at the paraxial focal plane is 1.1 acoustic wavelengths and the acoustic field strength falls off on either side of the paraxial focal plane. In the longitudinal case the distribution at the paraxial focal plane (curve A) is not well focused as one would expect by considering the geometrical aberrations of Eq. (10). It is found, however, that a reasonable focus does exist at a plane 4 acoustic wavelengths closer to the acoustic lens. The attainable resolution for the longitudinal wave case will be nearly a factor of two less than for the shear wave case due to the wavelength difference (i.e., longitudinal velocity equals 5.79 km/sec and shear velocity equals 3.1 km/sec). It can also be seen by comparing the shear and longitudinal wave case that the depth of focus is much greater for the shear eave case. This is due to the enhanced shear wave generation at the larger values of ϕ .

We are confident that this is a viable system and we will proceed during the next interval with an experimental demonstration.

(g) SOS Device Studies

A device with silicon-on-sapphire is shown in the images of Fig. 14. There we show the comparison of the optical and the acoustic images. The silicon epi-layer is about one micron in thickness, the source and drain

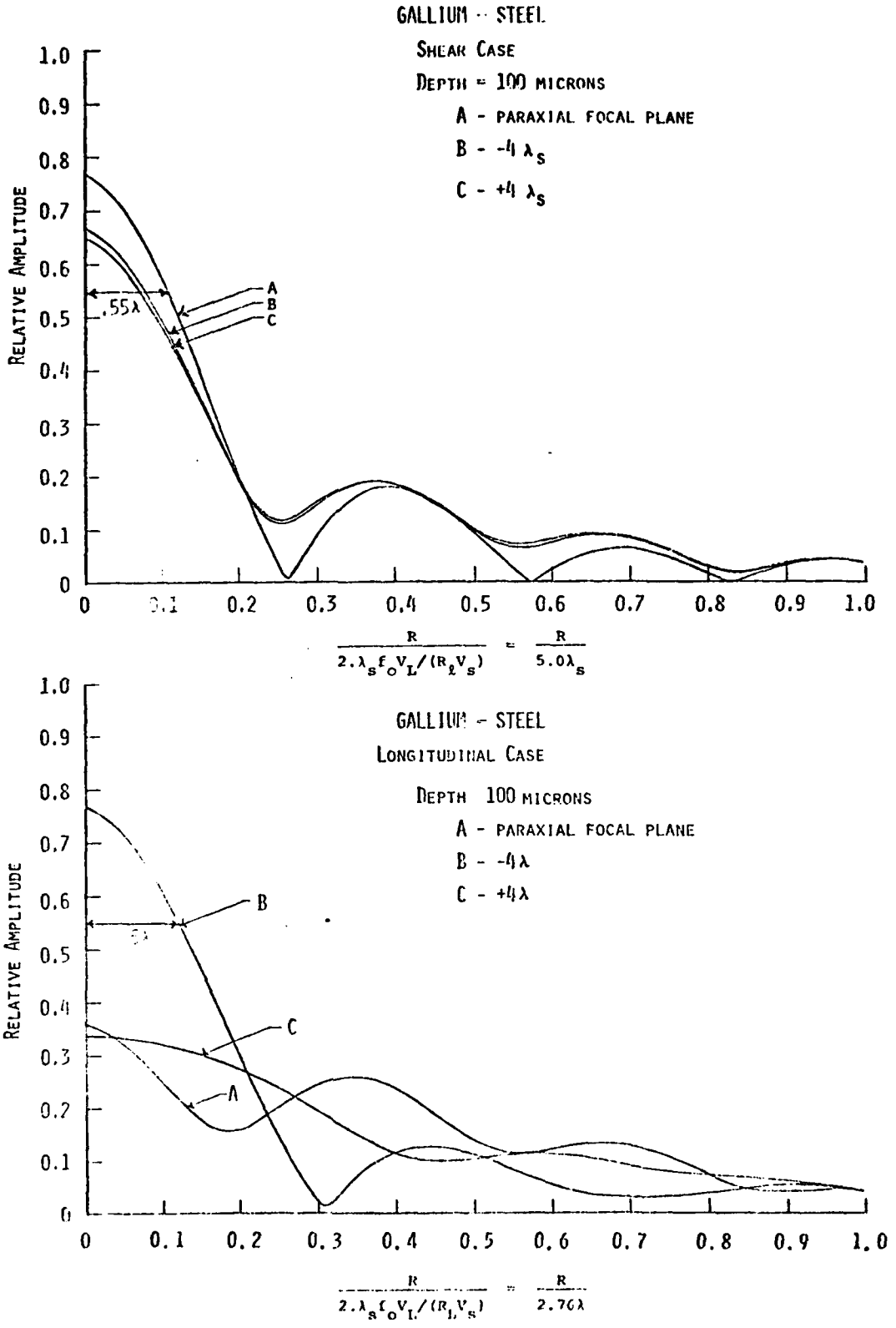

FIG. 13--Calculation of the acoustic field amplitude inside the solid for both the shear and longitudinal wave case. The maximum opening angle for the lens is 30 degrees.

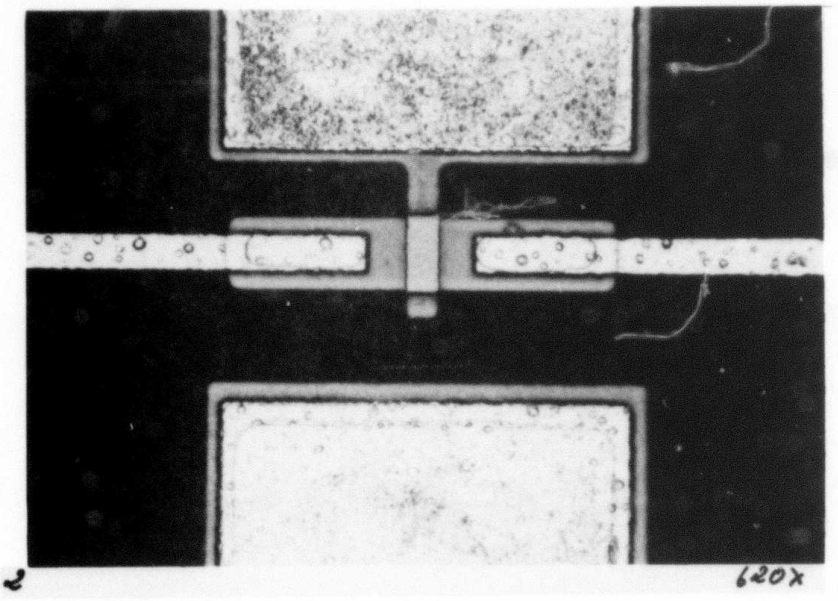

(A) Optical

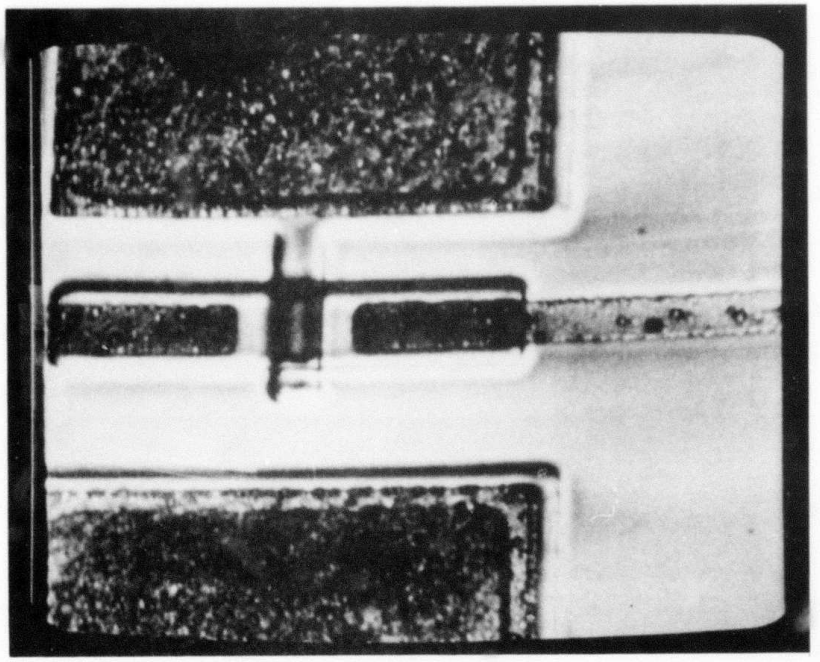

(B) Acoustic

FIG.14--MOS transistors - SOS technology (RCA)
Aluminum lines - polygate (5 μm).

contacts are aluminum, and the gate electrode is polycrystalline silicon. It is about 7 microns in width. The detailed acoustic images of two devices on the same wafer are shown in Figs. 15 and 16. We compare an optical close-up of the gate region with three acoustic images. The acoustic images are taken for three different spacings between the lens and the surface of the specimen. The "in-focus" image does not reveal a great deal more than is contained in the optical image but the other images do. In particular we find detail in the gate region which may be related to the electrical performance of the device. We know device A is defective in the sense that it has a large leakage current with reverse bias. Another presentation of this information for device A is presented in Fig. 17(g). There we scan a single line across the gate region and vary continuously, the spacing between the lens and the object. In that way we obtain a special kind of depth profile for this single scan line. Our interpretation of this display is not yet complete but we do have two conclusions. First, the sensitivity is extraordinary and second, the asymmetry in these images may relate to electrical performance. The sensitivity is such that a change of 0.3 microns in the lens-object spacing will produce a substantial change in the acoustic response at the acoustic image. This adjustment is so fine that we do not have a mechanical design that is fine enough to permit us to fully exploit this concept. The images in the x-y plane for the various focal distances are shown in Fig. 17 (a) through (f). This study will be continued into the next interval.

(h) Additional Studies of Silicon Integrated Circuits

We have continued our study of circuits integrated on silicon with the images of Fig. 18. The optical image is shown for comparison. This circuit was fabricated by Rick Davis at Stanford. It is interesting to us because

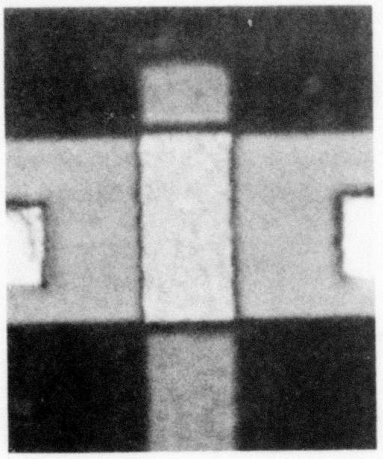

(a)

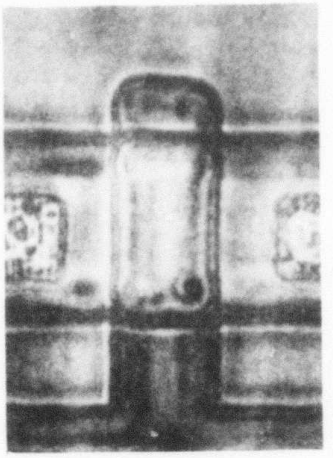

(b) +3.0

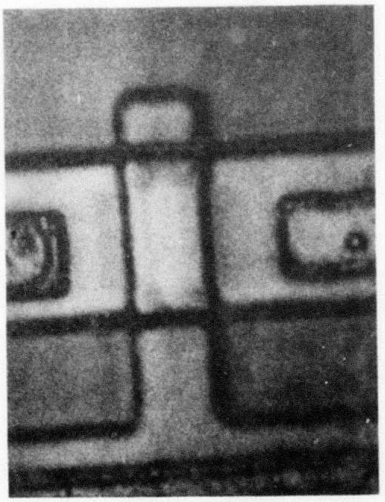

(c) 0

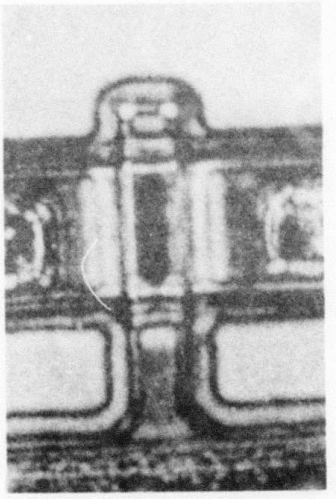

(d) -4.0

DEVICE A

FIG. 15--The gate region of an SOS transistor. (a) Optical image, (b), (c) and (d) acoustic images for in-focus (c). The lens-sample spacing is increased by 3 μm in (b) and decreased by 4 μm in (d).

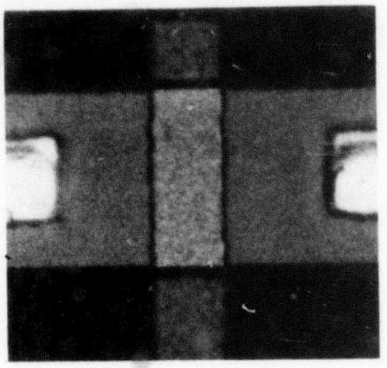

(a)

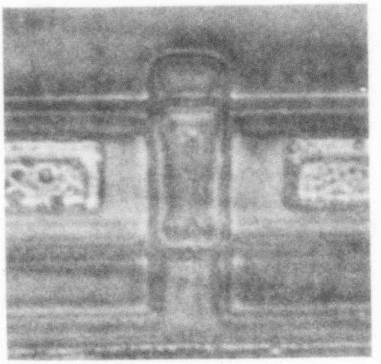

(b) +3.0

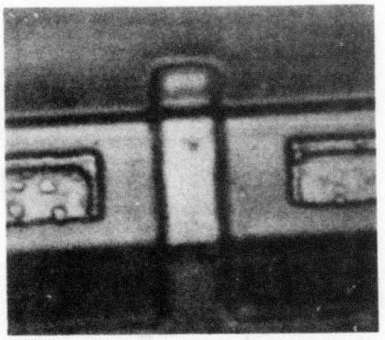

(c) + 1.0

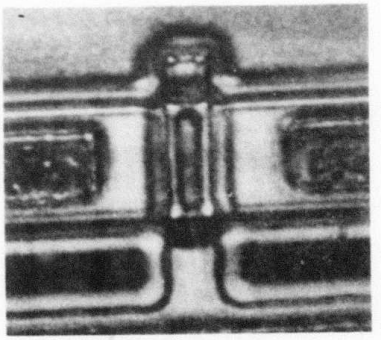

(d) -2.0

DEVICE #8

FIG. 16--SOS transistor with optical image in (a). The three acoustic images with the lens-sample spacing increased beyond the focal plane by 3 μm in (b), 4.0 μm in (c) and decreased by 2 μm in (d).

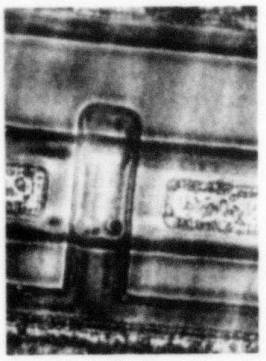

(a)

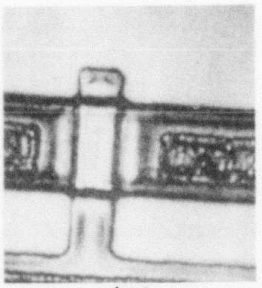

(b)

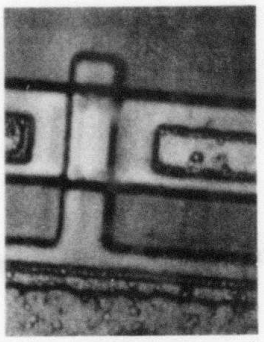

(c)

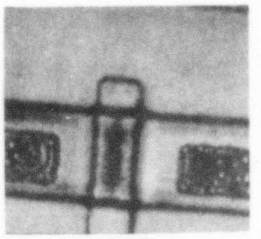

(d)

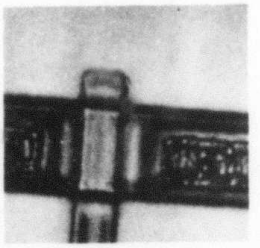

(e)

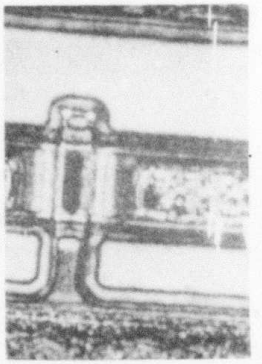

(f)

DEVICE A

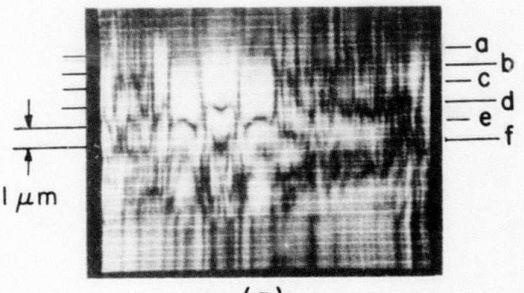

(g)

FIG. 17--The gate region images for various focal positions (a) through (f). In (g) we find the A trace for one position through the gate region plotted as a function of the lens-sample spacing.

(a)

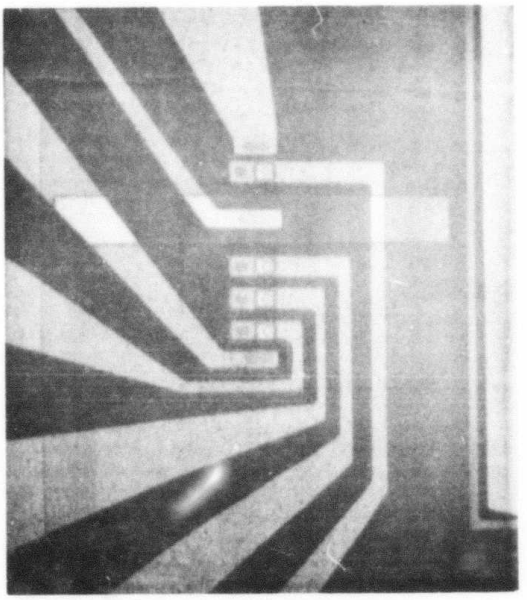

(b)

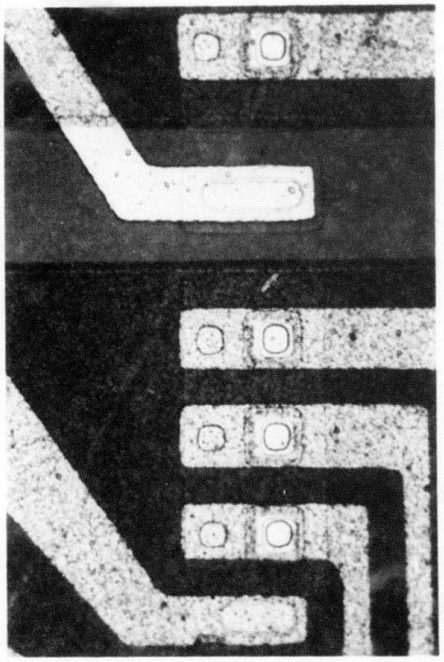

(c)

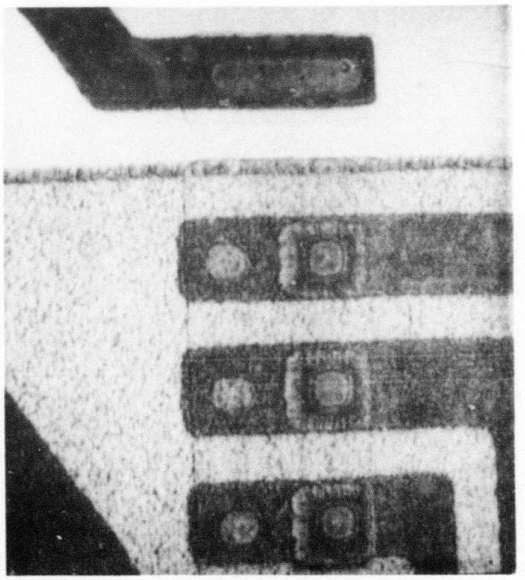

(d)

FIG. 18--The comparison of the silicon device of Rick Davis. (a) and (c) are optical, (b) and (d) are acoustic. The aluminum lines are on top of a polycrystalline silicon layer except for the smooth horizontal bar which is epitaxial silicon.

of the large areas of polycrystalline silicon under the metal lines. In Fig. 19 we show two enlarged acoustic images. The reversal in contrast results from the different focal position of the sample. It is a transistor with several gates used in logic circuits. The various levels show up with excellent contrast in the acoustic images.

In conjunction with Bob McDonald and Gene Meieran of Intel Corporation, we have been studying the acoustic response and images of various photoresist patterns as laid down on silicon wafers. This is recognized as an important element in silicon technology. Our interest centers on the high contrast that is available in the acoustic images (Fig. 20). It is higher than the optical contrast (Fig. 21) and it should, in principle, allow us to study properties of the photoresist layers with more detail than optically. The comparative images of photoresist patterns on silicon as included with Figs. 22 and 23 serve to emphasize these observations.

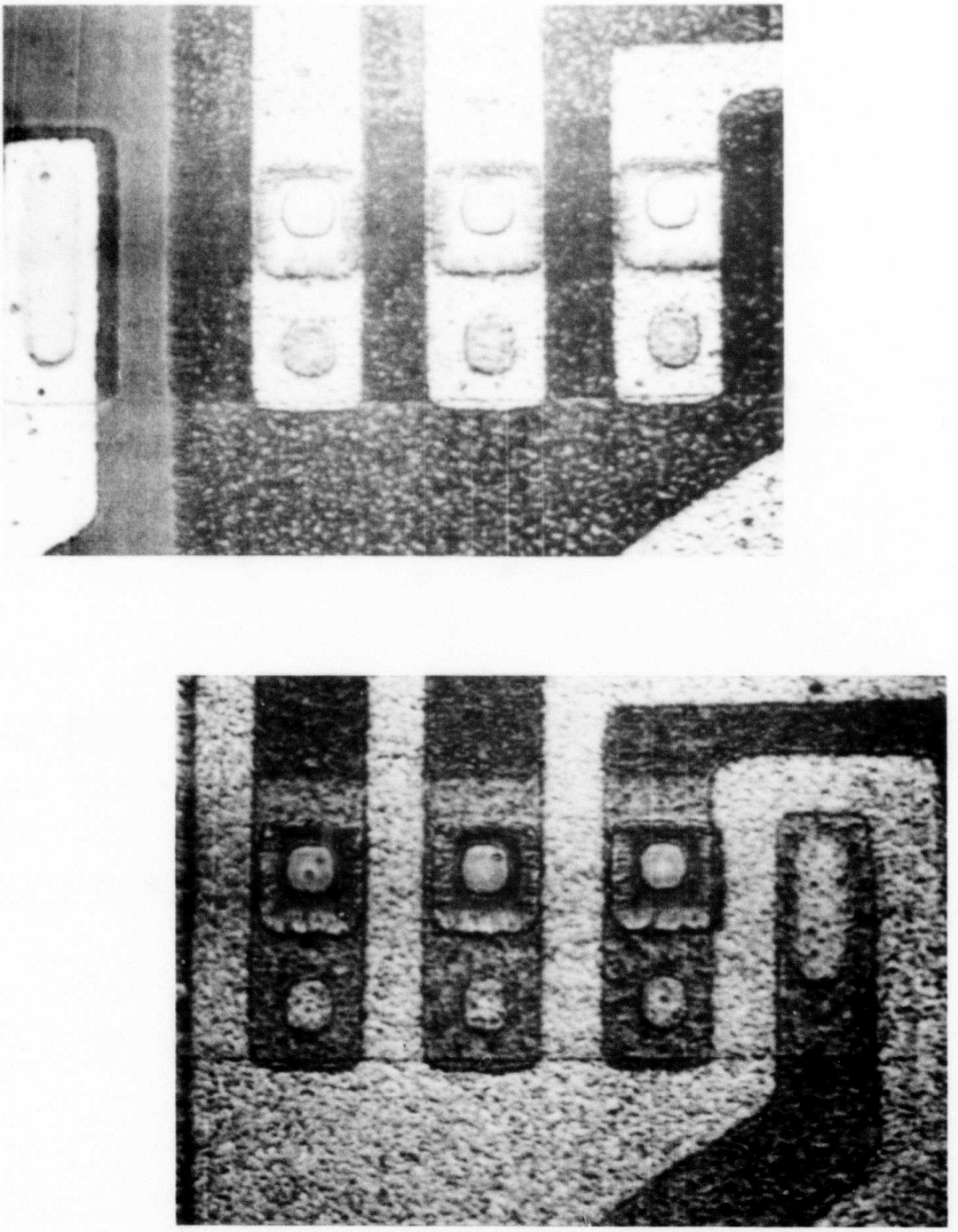

FIG. 19--The acoustic images of a silicon integrated circuit. The reversal in contrast comes from a change in the focal position of the sample. The metal lines are aluminum on a polycrystalline layer except for the left hand smooth portion which is epitaxial silicon.

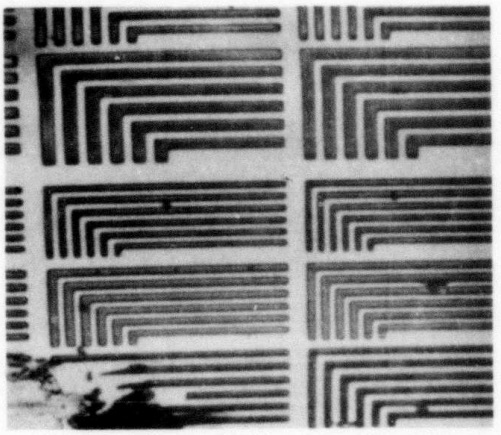

(a)

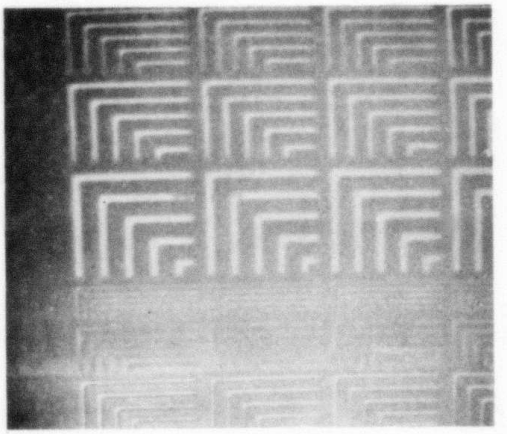

(b)

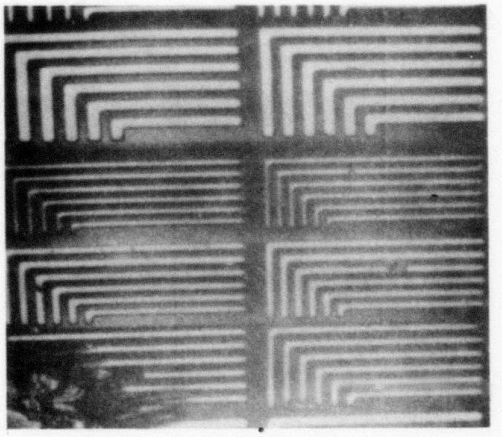

(c)

FIG. 20--The acoustic images of various photoresist patterns on silicon.

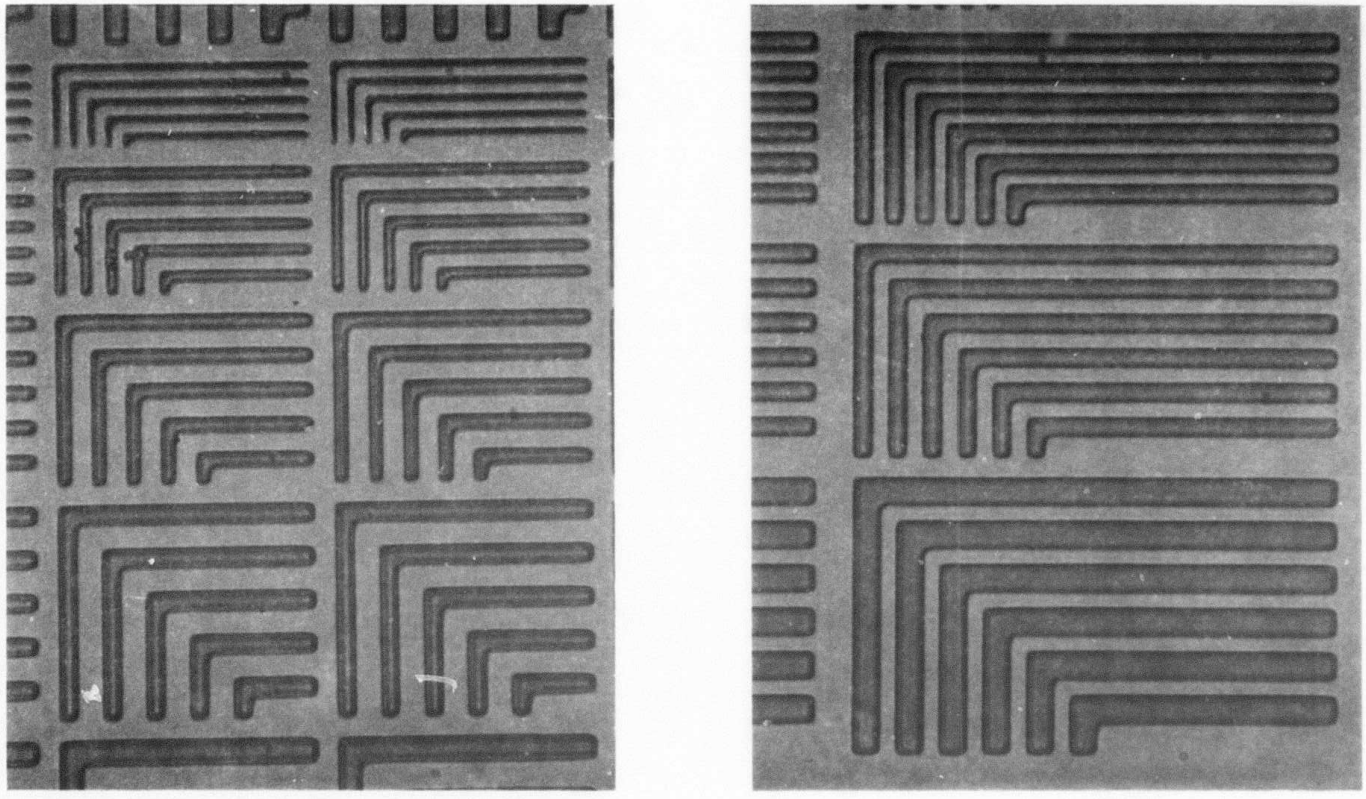

FIG. 21 The optical images (X1000) of the photoresist patterns on silicon. (Courtesy of Intel Corporation).

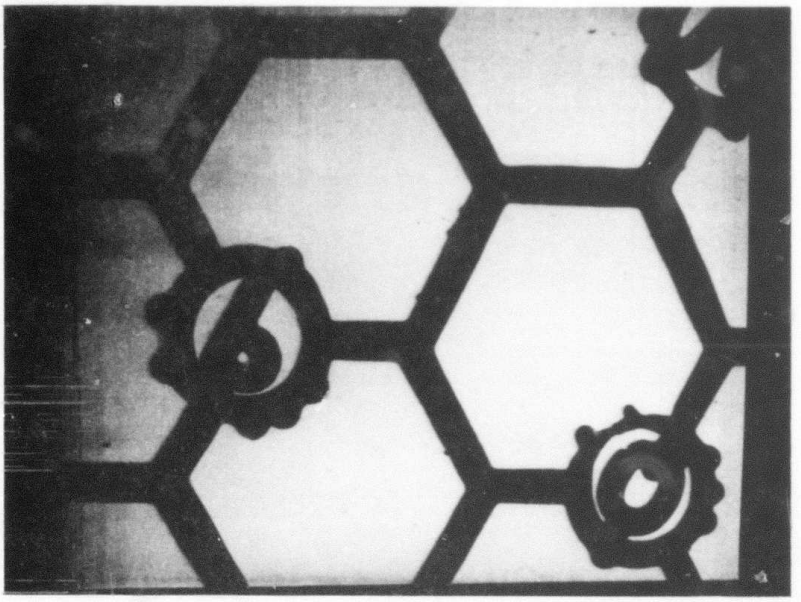

(a)

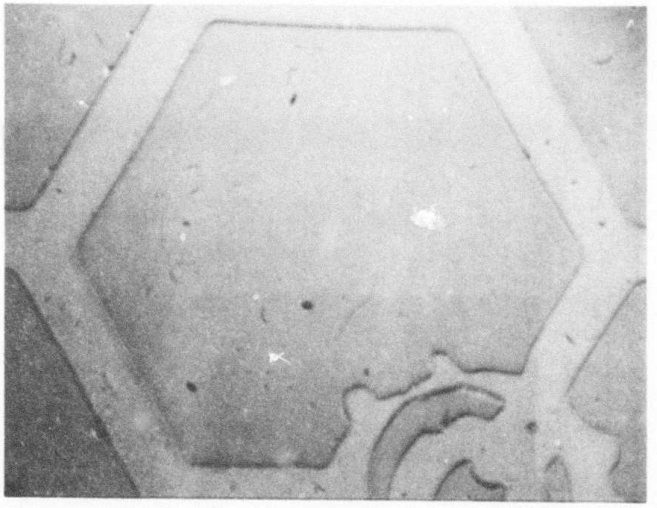

(b)

FIG. 22--The comparison of the acoustic (a) and optical (b) image of a photoresist pattern on silicon.

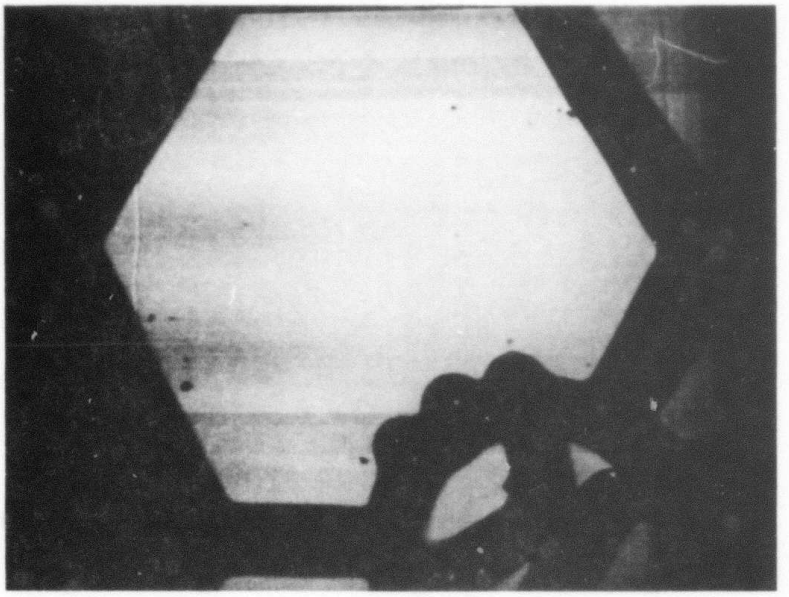

(a)

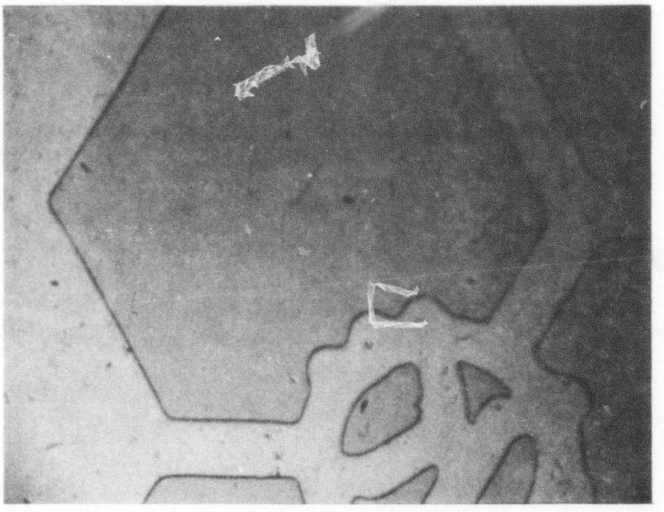

(b)

FIG. 23--Similar to Fig. 22 - photoresist on silicon.
Acoustic (a) and optical (b).

III. ADDITIONAL ACTIVITIES

There have been a substantial number of visitors during this interval ranging from groups who want to use the instrument to further their own research, to those who want to consider the possibility of making commercial instruments. The list includes:

Dr. Dick A. Bergren & Dr. Joseph A. Zelik, Hughes Aircraft Company, Culver City

Dr. Seymour Keller, IBM, Thomas J. Watson Research Center, Yorktown Heights

Dr. Francois Padovani, Texas Instruments, Inc., Dallas

Group from Olympus Optical Company, Tokyo

Dr. Robert J. Hessler, Cameca Instruments, Inc., Stamford

Dr. Ralph Hollis, IBM, Yorktown Heights

Dr. Graydon B. Larrabee & Dr. Philip F. Kane, Texas Instruments, Inc., Dallas

Dr. Noriyoshi Chubachi, Institute of Electrical Communication, Tohoku University, Sendai

Mr. Shosuke Soeda, Alps-Nortoronics Co. Inc., Sendai

Dr. Loomis, Loomis, Inc., Napa

Dr. William E. Ham, RCA, David Sarnoff Research Center, Princeton

Dr. Fred Gamble, Exxon Corporation, New Jersey.

The Principal Investigator has presented a number of invited talks in addition to the publications as listed. These include an invitation to talk at the International Symposium on "Electronic Imaging", sponsored by the Rank Prize Funds at the Royal Society in London, in September 1978. This talk will be included in the book to be published by Academic Press (London) Ltd.,

in 1979. We were invited by the Optical Society of America to present our work at their Annual Meeting in San Francisco in November 1978. In January 1979, we presented an invited colloquium at the Sandia Laboratories in Albuquerque, New Mexico.

Publications

A. Atalar, "An Angular-Spectrum Approach to Contrast in Reflection Acoustic Microscopy", J. Appl. Phys. 49, 5130-5139, October 1978.

H. K. Wickramasinghe, R. C. Bray, V. Jipson, C. F. Quate, and J. R. Salcedo, "Photoacoustics on a Microscopic Scale", Appl. Phys. Lett. 33, 923-925, 1 December 1978.

Preprints

C. F. Quate, "Ultrasonic Imaging", presented at the Rank Prize Funds International Symposium on "Electronic Imaging", London, England, September 1978, to be published by Academic Press (London) Ltd. in 1979.

A. Atalar, V. Jipson, R. Koch and C. F. Quate, "Acoustic Microscopy with Microwave Frequencies", to be published in Annual Review of Materials Science, vol. 9, August 1979.

C. F. Quate, A. Atalar and H. K. Wickramasinghe, "Acoustic Microscopy with Mechanical Scanning - a Review", Proceedings of the IEEE, to be published in August 1979.